Stress and Redox-dependent Chaperone Interactions in the Endoplasmic Reticulum in Barrett's Oesophagus

SIMPSON, LEE,DAVID

Stress and Redox-dependent Chaperone Interactions in the Endoplasmic Reticulum in Barrett's Oesophagus

A thesis submitted for the degree of Master of Science (Research)

Lee Simpson BSc
University of Durham
Van Mildert College
Submitted: 2018
Supervisor: Dr Adam Benham BA (Oxon), PhD

Acknowledgements

I would like to thank Dr Adam Bentham and Helen Lake for keeping me going and all the support they have granted me. If it wasn't for them this thesis wouldn't have been completed.

I would also like to thank Mr Viswanath YKS for his co-supervisory advice and James Cook University Hospital for their support and collaboration with this project.

I would like to thank the Barrett's support group for helping me fund this thesis and finally, I would like to thank Naomi, Matilda, Ben and Steven for their advice and support throughout.

Abstract

Barrett's Oesophagus (BO) is an acquired condition which alters the normal structure of the distal oesophagus. BO is important as it is the only known precursor lesion for Oesophageal Adenocarcinoma (OAC) with an annual conversion rate of approximately 0.3%. There is a strong correlation between acid-reflux and the development of BO, with patients with BO having a high incidence of bile acids in their refluxate, bile acids have been implicated in ER stress and disruption of protein folding which may be important in the transition from BO to OAC.

Over-expression GP-2 has been shown to protect oesophageal cells from bile acid induced stress. However, there is evidence to suggest that GP-2 is down regulated by hypermethylation of its promoter in BO. Prdx6 also has an antioxidant role but has not been investigated fully in BO and OAC. Finally AGR2 is a member of the PDI family which has been implicated in a number of cancers and may play a role in the development of OAC.

This thesis did not find any noticeable expression of GP-2 in OE cells or in tissue samples of BO and OAC. Western blotting of OE cells showed a difference in redox poise between OE19 and OE33 cells and IHC showed expression of Prdx6 is gastric-like cells in BO but none in OAC tumour cells. AGR2 did not appear to be expressed in the normal oesophagus but was present in gastric-like secretory cells in BO which appeared to remain closely associated with tumour cells in OAC. Cellular experiments showed that AGR2 forms redox dependant interactions within OE cells. Taken together this may suggest a relationship between Prdx6 and AGR2 and the transition of BO to OAC.

Contents

Abbreviations

AGR2	Anterior Gradient Protein 2
BCA	Bicinchoninic Acid
BIP	Binding Immunoglobulin Protein
BO	Barrett's Oesophagus
BSA	Bovine Serum Albumin
CALR	Calreticulin
CANX	Calnexin
cDNA	Complementary Deoxyribonucleic Acid
CLAP	Chymostatin, Leupeptin, Antipain, and Pepstatin A
DAB	Diaminobenzidine
DAPI	4',6-diamidino-2-phenylindole
DFOM	Deferoxamine mesylate
DIA	Diamide
DMEM	Dulbecco's Modified Eagle's Medium
DNA	Deoxyribonucleic Acid
DTT	Dithiothreitol
EDTA	Ethylenediaminetetraacetic Acid
ER	Endoplasmic Reticulum
ERO	Endoplasmic Reticulum Oxireductin
FAD	Flavin Adenine Dinucleotide
FBS	Foetal Bovine Serum
GPX	Glutathione Peroxidases
GORD	Gastro-oesophageal reflux disease
GPx	Glutathione Peroxidase
GSH	Glutathione
Hh	Hedgehog signalling
HRP	Horseradish Peroxidase
INM	Inner Nuclear Membrane
MEM	Minimal Essential Medium
NEM	N- ethylmaleimide
OAC	Oesophageal Adenocarcinoma
ONM	Outer Nuclear Membrane
OR	Odds Ratio
OSCC	Oesophageal Squamous Cell Carcinoma
PBS	Phosphate Buffered Saline
PDAC	Pancreatic Ductal Adenocarcinoma
PDI	Protein Disulphide Isomerase
PDIp	Protein Disulphide Isomerase pancreas
Prdx4	Peroxiredoxin IV
QSOX	Quiescin-sulfhydryl oxidase
RE	Reticulum
rER	Rough Endoplasmic Reticulum
RNA	Ribonucleic Acid
RNC	Ribosome Nascent Chain Complex
RNS	Reactive Nitrogen Species

ROS	Reactive Oxygen Species
RPMI	Roswell Park Memorial Institute
RTU	Ready To Use
SDS-PAGE	Sodium Dodecyl Sulfate Polyacrylamide Gel Electrophoresis
sER	Smooth Endoplasmic Reticulum
SHMs	Somatic Hypermutations Hotspots
SR	Signal Recognition Peptide Receptor
SRP	Signal Recognition Peptide
UPR	Unfolded Protein Response

List of Figures and Tables

Introduction

1.1 The Structure and Histology of the Oesophagus

The oesophagus is a muscular tube which begins at the pharynx and ends at entrance to the stomach comprising, from the outside in, of two muscle layers, longitudinal and circular, a submucosal layer, the muscularis mucosa layer, the lamina propria and finally the epithelial layer. The epithelium of the oesophagus consists of a stratified layer of squamous epithelial cells, containing small ducts linked to lubricant secreting, submucosal glands and changes to a non-stratified columnar epithelium at the gastro-oesophageal junction (Kershav, 2004).

Viewed histologically, the epithelial cells, at the luminal edge of the oesophageal epithelium, appear flattened, becoming gradually larger as the cells transition towards the basal zone, many of these cells are rich in glycogen. The basal zone of the oesophageal epithelium comprises of a variable number of layers of rectangular or cuboidal cells which lack glycogen and is scattered with melanocytes and neuroendocrine cells. Below the oesophageal epithelium is the lamina propria. The interface, between the basal epithelial layer and the lamina propria is irregular and tongues of the lamina propria extending towards the luminal surface. The lamina propria consists of a glycosaminoglycan matrix in which fibroblasts and loosely arranged collagen fibres are embedded, along with lymphocytes, eosinophils and occasionally plasma cells and mast cells. The muscularis mucosae, below the lamina propria, is variable in thickness, being thicker towards at the oesophageal-gastric junction. The muscle fibres of the muscularis mucosae, appear to be arranged irregularly in the upper portions of the oesophagus transitioning to continuous sheets of longitudinal and circular smooth muscle in the lower third (Stevens & Lowe, 1997).

1.2 Barrett's Oesophagus

Barrett's Oesophagus (BO) is an acquired condition which alters the normal structure of the distal oesophagus. In BO the stratified squamous epithelium of the oesophagus, near the oesophageal-gastric junction, is replaced by a metaplastic columnar epithelium which can comprise three different morphologies. These are; atrophic gastric-fundic type epithelium containing parietal and chief cells; transitional epithelium with cardic-mucus secreting glands and specialized columnar epithelium with intestinal-like goblet cells. However, there is some disagreement in clinical practice as to what constitutes BO. American gastroenterologists require the presence of specialised columnar epithelium for a positive diagnosis of BO, whereas British guidelines consider the possibility of diagnosing BO on the presence of gastric metaplasia only (di Pietro, et al., 2014).

BO, in itself is relatively benign and could be considered as an adaptive mutation in response to refluxing gastric contents, containing acid and bile. Ostrowski et al., utilising a genomic and proteomic approach discovered that there were over 2922 genes differentially expressed between 23 paired samples of Oesophageal squamous epithelium and BO samples including heat shock proteins and those that reflected defence, such as MUC1 and MUC5AC and repair, such as TFF2. (Ostowski, et al., 2007). Clinically, BO is important as it is the only known precursor lesion for Oesophageal Adenocarcinoma (OAC) (di Pietro, et al., 2014); (Watson & Galloway, 2014).

Oesophageal cancer is the 7th most common cancer in men, the14th most common in women (di Pietro, et al., 2014) and has shown an approximate 8-fold increase in incidence over the last three decades (Watson & Galloway, 2014). Oesophageal

cancer is aggressive in nature and is relatively asymptomatic in its early stages which results in a late diagnosis, resulting in Oesophageal cancer being the 4th and 7th highest cause of cancer related deaths in men and women respectively with a 5year survival rate of 5-10% (El Pietro, et al., 2014) (Watson & Galloway, 2014). Suffers of BO have a 0.3% annual conversion rate to OAC however there has been an increase in the incidence of BO and a decrease in age of presentation. According to the United Kingdom Barrett's Oesophagus Registry (Watson, 2014) 27% of the 12,000 registered BO suffers were diagnosed before the age of 55 (Watson & Galloway, 2014).

The development of BO into OAC is thought to be a multi-step process where the metaplastic, BO epithelium is thought to sequentially transition through a low grade dysplastic epithelium, to a high grade dysplastic epithelium and finally into invasive OAC (To, et al., 2016). The underlying mechanisms which drive the transition are unclear. One possible theory proposed is transdifferentiation, a change of one cell type into another. The early developing Oesophagus is composed of simple columnar cells which differentiate into the normal squamous epithelium during development. As the oesophagus develops the appearance of squamous epithelial cells coincides with the down regulation of Hh signalling, which transmits the information required by embryonic cells for proper differentiation. Wang D et al proposed that Oesophageal injury from acid and bile reflux could cause aberrant re-activation of the Hh signalling pathway and this could be the cause of the transdifferentiation to columnar cells in BO. Wang et al showed that over expression of Sonic Hedgehog in mouse Oesophagus epithelium instuces columnar gene expression, In addition Wang et al found 70 cases of BO with activated Hh signalling and so proposed that aberrant re-activation of the Hh signalling pathway

could be the cause of the transdifferentiation to columnar cells in BO (Wang, et al., 2010).

While transdifferentiation explains the observed replacement of the normal squamous epithelium with columnar epithelia, which is seen in BO, it fails to explain the rise in other cell lineages seen in BO. Given that the cell types observed in BO resemble those represented in intestinal tissue it is possible that oesophageal stem cells undergo transcommitment into an intestinal type stem cells. The exact location of the stem cell which gives rise to BO is unknown although a number of candidates exist, namely squamous oesophageal stem cells in the basal epithelial layer, stem cells present in the submucosal glands (Burke & Tosh, 2012) and finally gastric stem cells which have migrated from the gastric cardia at the gastro-oesophageal junction (Quante, et al., 2012)

There is also evidence to suggest other possibilities. Wang et al showed that a discrete population of embryonic epithelial cells persist in adult mice and human at the squamous-columnar junction and can migrate to the site of squamous epithelial injury and populate (Wang, et al., 2011). Additionally, a rat model of Reflux Oesophagitis (RO) showed evidence that multi-potential stem cells migrated from bone marrow via the blood to the site of the reflux-damaged-epithelium (Sasoi, et al., 2008).

Whilst environmental and lifestyle factors, appear to be a major correlative factor in the development of BO (Table 1.1) there appears to be some evidence of a possible genetic relationship in the development of BO and OAC. Studies have shown that within different populations of BO and OAC approximately 7% of sufferers show some familial clustering (Pesto, et al., 2014).

Table 1.1: Risk Factors for the development of Barrett's Oesophagus (El Petros, et al., 2016) (Njeuchkin & Souza, 2016) (Easterly & Saxe, 2014)

Risk factor	Barrett's Oesophagus Association
Chronic Heartburn, Erosive Oesophagitis or Symptoms of Gastro-Oesophageal reflux and higher in patients with an extent of reflux >30 years of age	Strong association, particularly with longer BO segments
Obesity particularly in people with a high ratio of Abdominal fat compared to subcutaneous	Strong association, increasing with BMI and waist circumference
Smoking status	Some association. Differing studies conflict on the association with smoking and BO. Strong association in OAC with a dose-response relationship. Still elevated in ex-smokers but decreasing with cessation period
Gender, Race and Age	Higher male to female association and more prevalent in Caucasians, risk increases with age
Diet	Increased risk associated with low vegetable consumption and high consumption of red and processed meats.
Genetic Factors	An increased risk has been associated with a familial history of BO and or OAC
Pregnancy Complications	There is some association with the development of BO and low birth weight but not with the development of OAC. Conversely premature birth is associated with an increased risk of OAC but not BO.

A number of genome wide association studies have identified loci that correlate with increased disease risk, the most notable of which are described below.

The Esophageal Adenocarcinoma Genetics Consortium tested over 521,000 single nucleotide polymorphisms (SNPs) and discovered an association with a SNP on chromosome 6p21 within the major histocompatibility complex, odds ratio (OR) (95% confidence Interval (CI)) of 1.21 and a SNP on chromosome 16q24 OR (95%CI) of 1.14, which codes for FOXF1, a protein thought to be associated with Oesophageal development (The Esophageal Adenocarcinoma Genetics Consortium and the Wellcome Trust Case Control Consortium , 2012). Another group headed by David Levine found three possible SNPs, 16p13 (CRTC1) associated with oncogenic activity when aberrantly activated, 6q22 in BARX1 a transcription factor related to oesophageal specification and FOXP1 on 3p14 a regulator of oesophageal development (Levine, et al., 2013). Whatever the driver of the change in BO there appears to be evidence of a progressive increase in mutational load with a subsequent accumulation of general genomic instability and oncogenic events such as the loss of the tumour suppressor genes CDKN2A and TP53 (Ross-Innes, et al., 2015) (Stachler, et al., 2015).

Although there is evidence of a genetic subset of people who are at an increased risk of the transition of BO to OAC, one of the main risk factors for BO appears to be the presence of acid reflux (Table1.1). Gastro-Oesophageal Reflux Disease (GORD) and erosive Oesophagitis are strongly correlated with the development of BO. Fass et al found that 12% of those presenting with GORD and 36% of those with Oesophagitis had BO. Additionally they demonstrated that the length of BO

segments correlated with the exposure to acid in the Oesophagus. They found that patients with shorter segments of BO experienced significantly less exposure to reflux acid than those with longer segments of BO both when upright or supine, concluding that duration of acid exposure is an important factor in determining the length of the Barrett's mucosa (Fass, et al., 2001). There appears to be a strongly correlated link between increased acid reflux and BO and patients with BO have a high incidence of bile acids in their refluxate (Fujimura, et al., 2011) implicating bile acids as etiologic agents in cancers of the gastrointestinal tract (Bernstein, et al., 2009). Ducrak et al demonstrated that a bile acid cocktail, comprising of the sodium salts of glycocholic acid, taurocholic acid, glycodeoxycholic acid, glycochenodeoxycholic acid and deoxycholic acid, acidified to pH4 could induce oxidative stress in Human Barrett's Oesophagus tissue. In addition they showed that the combination of bile acids and low pH caused an increase in oxidative stress and oxidative DNA damage, shown by an increase in 8-hydroxy-deoxyguanosine, a marker for oxidative DNA damage in BO, Seg-1 and HET-1A cells (Ducrak, et al., 2007). The bile salt deoxycholic acid has also been implicated as a carcinogen in gastrointestinal cancer by indirectly damaging DNA through the production of reactive oxygen and reactive nitrogen species (ROS/RNS) (Bernstein, et al., 2005) and with oxidative and Endoplasmic Reticulum (ER) associated stress, protein misfolding and calcium ion (Ca^{2+}) imbalances in human cholestatic liver disease (Bernstein, et al., 1999). These associations suggests that acid reflux and its effects on the ER , may be important in the transition from BO to OAC.

1.3 The Endoplasmic Reticulum

The Endoplasmic reticulum (ER) is a continuous membrane system, interconnected with the nuclear envelope (Figure 1.1). It is comprised of a single membrane bilayer, forming a single continuous lumen which has various domains that perform different functions, including protein synthesis, folding, transport to the Golgi and lipid biogenesis (Schwarz & Blower, 2016). The ER is continuous with the nuclear envelope (NE) and consists of two main domains, the rough endoplasmic reticulum (RER) and the smooth endoplasmic reticulum (SER). The NE surrounds the nucleus, it consists of an inner nuclear membrane (INM) and an outer nuclear membrane (ONM). These are large cisternal membranes separated by the inter nuclear membrane space (English & Voeltz, 2013). The NE acts as a barrier to selectively control the entry and exit of molecules to the nucleus. Transport of molecules between the nuclear and cytoplasmic compartments is facilitated by nuclear pore complexes that bridge the INN and ONN (Schwarz & Blower, 2016). The ER branches out from the ONM as an interconnected network of cisternae comprising the RER and the SER (Figure 1.1) with the conformationally stacked, flat cisternae of the RER localised nearest the NE (Schwarz & Blower, 2016) (English & Voeltz, 2013). The RER comprises of two lipid bilayers with an intervening lumen which varies in size. The luminal space is consistently around 50 nm in mammals and 30 nm in yeast (Schwarz & Blower, 2016) and the sheets of the RER are connected by helicoidal membrane motifs (Terasaki, et al., 2013). The RER is defined by the high density of ribosomes on its cytosolic surfaces and its function is the synthesis, folding and modification of proteins destined to be secreted or membrane bound (Schwarz & Blower, 2016).

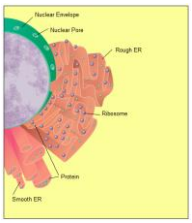

Figure 2.1 The Endoplasmic Reticulum. A graphical representation of the ER. The ER abuts the Nucleus and is composed of two defined types: the rough ER and the smooth ER. The rough ER is studded with ribosomes, where membrane-destined proteins are positioned along the rough ER. Adapted from (Mariani, 2016)

The SER comprises a highly curved and smooth network of interconnected tubules and is defined by the lower density of ribosomes (English& Voeltz, 2013). The SER is highly dynamic and constantly rearranging and is considered to be the primary site of Lipid biogenesis (Schwarz & Blower, 2016).

1.4 Protein entry into the Endoplasmic Reticulum

A newly synthesised, nascent protein chain exists in a conformation determined by its amino acid sequence. Many nascent proteins, in order to assume a form that is biochemically active, must undergo some form of protein folding and this process must be reproducible in order that every protein translated from a particular mRNA sequence results in a form fit for purpose.

Proteins that are expressed at the cell surface, are part of the secretory pathway or are destined to be secreted are targeted to the ER by a signalling sequence which is located at the N-terminus of the emerging nascent polypeptide chain (Figure 1.2). This signal sequence is usually around 25 amino acids in length and comprises of 8-12 hydrophobic amino acids preferentially formed in an α-helix the exact composition of which is variable in length, shape and amino acid composition (Heijne, 1985). This signal sequence binds to a Signal Recognition Particle (SRP), which facilitates the targeting of the translating protein to the ER membrane (Figure 1.2A) (Frost, 2005). The SRP is a ribonucleoprotein complex comprising of, in mammals, a 7SL RNA of approximately 300 nucleotides, formed into a double stranded secondary structure in complex with six protein subunits (SRP 9, 14,19, 54, 68 and 72) and can be thought of as consisting of two structural domains, named the Alu and the S-domain (Walter & Blobel, 1982). The Alu-domain is made up from helices 3-5 of the 7SL RNA and SRP 9 and 14 subunits.

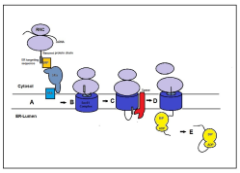

Figure 1.2 Co-Translocation of Na-scent Proteins into the Endoplasmic Reticulum. The nascent protein chain ER targeting sequence emerges from the Ribosome Nascent Chain Complex (RNC), arresting Translation. The Signal Recognition Particle (SRP) associates with the ER localization sequence+. This targets the nascent protein to the ER by binding to the SRP receptor (SR) on the surface of the ER [A], the SR unwinds at an a and β subunit, binding to the SR [B]. Translation then resumes [C], the RNC docks with the Translocon (Sec61) and the nascent protein is translocated into the ER [D]. The nascent protein chain passes through the Sec61 complex as a loop [D], the ER targeting sequence is swiped by Signal sequence peptidase complex (Spase). . SIP binds to the nascent chain, in an ATP dependant manner [E] and the nascent chain is released from the RNC and is chaperoned to folding in the ER [E]. [reversed in (Zimmermann, et al., 2011)]

The S-domain comprises of the rest of the 7SL RNA and the SRP19, the SRP54, the SRP68 and the SRP72 protein subunits. Of all the subunits SRP54 is key to the function of the SRP, in that it is involved in interaction with the ribosome, signal sequence recognition and interaction between the SRP and the ER membrane SRP-receptor (SR) (Nyathi, et al., 2013). Structurally SRP54 is comprised of 3 main domains an α-helical, methionine rich domain (M) located at the C-terminus; a GTPase domain (G) and a N-terminal helical domain (N). The M domain binds the nascent chain signal sequence and the N and G domains are involved with in the interaction with the SR. The M and NG domains are joined by a highly conserved and flexible linker which permits the subunit to undergo structural rearrangement and allows communication between the domains (Nyathi, et al., 2013) (Halrorl, et al., 2011).

Unique to the eukaryotic SRP, binding of the signal sequence to the SRP14 subunit of the SRPs ALU domain, is capable of causing a transient arrest in the elongation of the nascent chain. Experiments with SRP mutants compromised in their ability to arrest elongation have demonstrated defects in translocation, suggesting that the arrest capability of the SRP could be to ensure that the nascent chain remains competent until the RNC has bound to the translocon (Nyathi, et al., 2013).

The SRP binds to the Ribosome Nascent Chain Complex (RNC) with low affinity. However, it is only the presence of an exposed signal sequence that leads to high affinity binding through the M domain of the SRP subunit of the SRP (Nyathi, et al., 2013). Binding of the signal sequence causes a conformational change in SRP54 which is thought to promote receptor engagement (Halrorl, et al., 2011).

Once formed the RNC-SRP complex is targeted to the ER membrane bound SR. The SR (Figure 1.2A) comprises of two subunits, namely SRα and SRβ. SRβ is a 30kDa integral membrane protein anchored to the ER membrane via a single transmembrane domain. SRα is a 70 kDa protein that is tightly bound to SRβ at its N-terminal SRX domain, its C-terminus region includes a GTPase domain and has a high homology with the NG domain of SRP54 (Nyathi, et al., 2013). SRα also has a GTPase domain that only interacts with SRβs SRX domain when it is in a GTP bound state. Schwartz and Blobel suggest that the GTP cycle of SRβ may control the association and dissociation of the SR (Schwartz & Blobel, 2003). The SRα subunit of the SR forms the interaction between the SR and the SRP. The NG domain of SRP54 forms a pseudo homodimer with the SRX domain only when the GTPase domains of both SRP54 and SRX have bound GTP (Nyathi, et al., 2013). There is also some evidence to suggest that kinetics of the formation of the SRP-SR complex provides some proof reading ability, in that only the binding of genuine ER targeting sequences to the SRP promote rapid and stable SRP-SR dimerisation (Zhang, et al., 2010).

Protein entry into the ER is facilitated by the Sec61 translocon complex (Figure 1.2B). The Sec61 complex is a heterotrimer of two highly conserved subunits α and γ and a less well conserved β subunit. The α subunit, which forms the pore that surrounds the translocating nascent chain during transfer across the ER membrane (Ng & Walter, 1996), has ten transmembrane (TM) domains and can be thought of as being in two distinct halves, TM 1-5 and TM 6-10. The TMs are arranged to form a central pore, with a cytosolic loop between TMs 5 and 6, which functions as a hinge allowing the opening of the pore. The luminal side is occluded by a plug

formed by a sub domain of the 2nd transmembrane domain. The γ subunit traverses the ER membrane diagonally across the back of the α subunit and has a role in opening the luminal side of the pore complex to allow protein entry in the ER lumen. The β subunit barely contacts the α subunit and its exact function has not been fully elucidated (Nyathi, et al., 2013).

Binding of the RNC to the Sec61complex (Figure 1.2) initiates opening of the pore complex and passage of the nascent protein chain into the ER lumen. Evidence suggests that the nascent chain signal sequence binds at the cytosolic side of the translocon and forms a hairpin-loop until the nascent protein is released from the RNC. The signal sequence can then be cleaved by signal peptide peptidases Spase. (Figure 1.2C) (Schau, et al., 1998). However there is also evidence that suggests that initially the signal sequence may be inserted head first into the pore, in this case at some point the signal sequence flips, inside the pore, into a hairpin-loop leading to the translocation of the c-terminal residues of the nascent chain and may require the interaction of accessory proteins Sec62p and ER[(Nyathi, et al., 2013) (Devarasent, et al., 2011). As translocation draws to completion, the nascent protein chain is chaperoned by the ER chaperone grp78 (BiP, Figure 1.2D) and post translationally modified, folded and stabilised by the addition of intramolecular disulphide bonds between chains of a single protein or intermolecular disulphide bonds between separate chains.

1.5 Oxidative Protein Folding in the ER

Disulphide bond formation is necessary to confer stability for secreted proteins, when they are exposed to the extracellular environment or, in the case of recycled

membrane proteins, passage through acidic endocytic compartments (Bulleid, 2012).
The formation of disulphides begins as a nascent protein chain is translocated in to the ER. The initial collapse of a nascent chain into its secondary structure brings cysteine residues close enough together for the formation of disulphide bonds. The lumen of the ER is a more oxidised environment than the cytosol and as such favours the oxidation of free thiol groups (-SH) and the formation of disulphide bonds (S-S). However, correct disulphide bond formation requires enzymatic help to promote bond formation between cysteine residues and to remove those disulphide bonds that may form during folding but are not required by the protein's final form (Bulleid, 2012) (Braakman & Bulleid, 2011). Central to this cycle of oxidation and reduction is the protein disulphide isomerase (PDI) family of enzymes (Bulleid, 2012).

The PDI family of enzymes have the ability to serve as molecular chaperones and to act as oxireductases and as isomerases, forming, breaking and rearranging disulphide bonds within their protein 'clients' (Figure 1.3A) (Benham, 2012). Formation of disulphide bonds requires that PDI family members be oxidised, there are a number of specific oxidases that, while being unable to introduce disulphide bonds themselves into client proteins, can specifically oxidise PDI family members (Bulleid, 2012), with the exception of quiescin sulfahyl oxidase (QSOX), a Golgi localised protein, which has been shown to be able to introduce disulphide bonds without the aid of additional partners. However, being localised to the Golgi apparatus it is thought not to be involved in oxidative protein folding (Chakravarthi, et al., 2007).

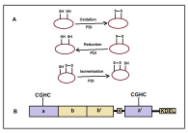

Figure 1.3 PDI A) Graphical representation of PDI's action on client proteins (not to scale). PDI can act as a catalyst with the ability to oxidize, reduce or isomerize disulphide bonds. B) PDI contains two catalytic a domains (a, a') and two non-catalytic b domains (b, b'). The a' and b' domains are connected by an X-linker region. The C-terminal KDEL mediates ER retention/retrieval. (adapted from *Kozlov, 2010* **)**

Structurally, the main building block of PDI is the thioredoxin domain. PDI contains two active thioredoxin domains a and a' as well as two inactive b and b' (Figure 1.3B). The b' and a' domains are separated by an x-linker region which contains a hydrophobic cap that can regulate ligand binding and homodimerisation (Bentham, 2012). The active sites of a PDI family member usually contain a CxxC motif, which is normally CGHC in PDI (Bentham, 2012). The intramolecular disulphide bond in the CxxC motif has a high reduction potential compared to that of unfolded client proteins allowing the ready donation of its disulphide bond to a protein with a reduced thiol (Bentham, 2012).

The mechanism of oxidative protein folding can be considered as a series of oxidation reactions between PDI family members and different oxidases. The main oxidase is ER Oxidoreductase 1 (ERO1) but both Glutathione Peroxidase 7/8 (GPx7/8) and Peroxiredoxin IV(Prdx4) have also been suggested as capable of oxidising PDI (Figure 1.4) (Sullivid, 2012). ERO1 and PDI form the main pathway for disulphide bond formation in the ER. ERO1 is a glycosylated flavoprotein associated with the luminal side of the ER membrane. It has two homologues, in *homo sapiens*, ERO1α and ERO1β (Sevier & Kaiser, 2008). These homologues appear to undertake similar functions but have different tissue distribution (Pagani, et al., 2000). ERO 1 has two catalytic sites each featuring a pair of cysteines. The 'active' site is located close to the bound FAD cofactor and the 'shuttle' site is located on a flexible loop. ERO1 promotes disulphide bond formation by utilising the oxidation potential of molecular oxygen and its bound FAD cofactor to generate internal disulphide bonds that it can transfer to the client protein via PDI. This is achieved by a series of thiol-disulphide bond exchange reactions (Figure 1.4A). Catalysis by ERO1 involves the direct oxidation of PDI by the shuttle site and the re-

oxidation of the reduced shuttle site by internal thiol-disulphide exchange between the shuttle and the active sites. Molecular oxygen and FAD in turn re-oxidise the active site producing H_2O_2 (Sullalid, 2012) (Sevier & Kaiser, 2008).

ERO1 is not the only ER resident protein that is capable of oxidase activity and has been found to interact with PDI. Both Nguyen et al and Wang et al have demonstrated that GPx7 and GPx8 have the ability, in the presence of H_2O_2 to oxidise PDI and facilitate disulphide bond formation in client proteins (Nguyen, et al., 2011) (Wang, et al., 2014). GPx7 and 8 are members of the GPx family.GPx7 is a soluble ER protein and GPx8 is a type 1 membrane protein (Sullalid, 2012). Nguyen et al demonstrated evidence that both GPx7 and GPx8 were ER localised glutathione peroxidases closely associated with ERO1 and neither demonstrated substantial glutathione peroxidase activity, instead they demonstrate PDI peroxidase activity.ie they show a preference for accepting electrons from PDI. *In vitro* studies demonstrated that addition of GPx7/8, PDI and peroxide to a reduced unfolded protein resulted in disulphide formation and rapid refolding into its native state. They also demonstrated that addition of GPx7/8 to a mix of PDI, ERO1α and reduced glutathione (GSH) resulted in a significant increase in oxygen consumption. Together this information provides evidence to suggest that GPx7 and Gpx8 form part of a pathway designed to efficiently utilise the peroxide produced by the main ERO1-PDI pathway for disulphide bond formation (Nguyen, et al., 2011).

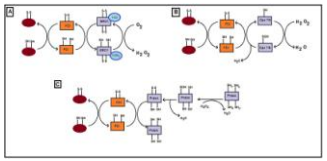

Figure 1.4 Mechanism of the interactions between the oxidase ERO1, GPx7/8 and PrxIv4. **A)** Thiol groups within ERO1 form a disulphide bond donating electrons to FAD which is reduced to $FADH_2$. PDI accepts electrons from ERO1, resulting in the oxidation of PDI and the reduction of the disulphide bond in ERO1 which it can then pass on to its client protein. Molecular oxygen acts as the ultimate electron acceptor regenerating FAD and producing H_2O_2. **B)** GPx7/8 utilises H_2O_2 resulting in the sulphenylation of the active cysteine which is reduced passing its sulphide to PDI, oxidising PDI and forming a disulphide bond that can be donated to a client protein. Finally, **C)** The third groups within PrxIv4 can be considered resolving and peroxidatic, in a similar way to GPx7/8 the first step is the utilisation of H_2O_2, for the sulphenylation of the peroxidatic cysteine within PrxIv4, this quickly interacts with a resolving cysteine forming a disulphide bond which is passed to PDI and ultimately from PDI to a client protein. (Bulleid, 2012) (Rancourt, et al., 2018) (Tavender, et al., 2010) (Wang, et al., 2012).

This evidence is further supported by Wang et al, who showed that GPx7 could utilise the peroxide generated by ERO1α to accelerate disulphide dependent protein folding both *in vitro* and *in vivo*. The mechanism by which, they suggest, GPx7 utilises H_2O_2 to oxidise PDI is shown in Figure 1.4B. As can be seen H_2O_2 oxidises a GPx7 cysteine, CysS7 to sulphenic acid. This can then either form an intra molecular disulphide bond with Cys86 or interact with PDI directly. They further suggest that ERO1, PDI and GPx7 form a triad which can utilise a single molecule of oxygen to produce two disulphide bonds and two molecules of H_2O (Wang, et al., 2014)

In addition to the evidence showing that GPx7 and 8 are capable of directly oxidising PDI to drive disulphide bond formation, evidence has also been presented to show that PrdxI has the capacity to directly oxidise PDI and drive disulphide bond formation in the presence of H_2O_2 (Tavender, et al., 2010). PrdxI is a member of the peroxiredoxin family, PrdxI contains an N terminal signal sequence which was thought to allow secretion but Tavender et al demonstrated that it was actually localised to the ER. PrdxI is considered a member of the typical 2-Cysteine (2-Cys) family of peroxiredoxins, in that in addition to its redox-active 'peroxidatic' cysteine it also contains an additional cysteine, known as the resolving cysteine near its C-terminus. Catalytic activity of these 2-Cys peroxiredoxins is facilitated by the formation of toroid-shaped decamers constructed of 5 catalytic dimers. Multimer formation provides the optimal arrangement of the peroxidatic cysteines to maximise catalysis. (Tavender, et al., 2008) (Wang, et al., 2012). PrdxI reacts as a scavenger of H_2O_2 in the ER (Wang, et al., 2012), where reaction with H_2O_2 causes the peroxidatic cysteine to become sulphenylated (Figure 1.4). Sulphenylation causes a conformational change within the PrdxI dimer which brings the resolving cysteine on

one chain in the dimer close to the sulphenylated peroxidatic cysteine on the other (Bulleid, 2012), destabilising the Prdx4 decamer complex in the process (Tavender, et al., 2008) and forming a disulphide bond (Figure 1.4). The formation of this disulphide allows the Prdx4 dimer to readily accept electrons from reduced PDI, oxidising the PDI active site to form a disulphide that can then be passed to a client protein (Tavender, et al., 2010) (Bulleid, 2012) removing ERO1 generated H_2O_2 and forming two disulphide bonds and water for the cost of a single reduced molecule of oxygen.

1.6 Disruption to Oxidative Protein Folding may result in ER stress and could contribute to the pathogenesis of Barrett's Oesophagus and Oesophageal Adenocarcinoma.

There exists a link between cellular damage or injury, oxidative stress and ER stress and perturbation of oxidative protein folding in the ER (Zhang, 2010) (Burton & Jauniaux, 2011). Bernstein *et al* demonstrated that exposure of HepG2 cells to the bile salt deoxycholate, induced the increased activation of promoters and transcription factors associated with the response to DNA damage (Gadd153, hsp70 and c-fos), oxidative stress (NF-κβ, Gadd153, hsp70 and c-fos) and those that respond to protein misfolding (grp78 and hsp70) and ER stress (grp78) (Bernstein, et al., 1999). The activation of grp78 in response to oxidative stress in a liver cancer cell line is a good indicator of the link between cellular stresses and ER stress, as grp78 is one of the main chaperones in the ER and increased expression is an indication of the activation of the ER unfolded protein response (UPR) which responds to an increase in misfolded proteins in the ER and drives the increase in

expression of components of the oxidative protein machinery (Schroder & Kaufman, 2005). Over-expression of grp78 is not restricted to cancers of the liver, Langer *et al* found that grp78 mRNA, which correlated with actual protein expression, was highly expressed in primary resected oesophageal adenocarcinoma tissue sections, particularly in early stage OAC (Langer, et al., 2008). There is also evidence that suggests that activation of Gadd153, by DNA damage and oxidative stress, sensitises cells to ER stress leading to a depletion of cellular glutathione (GSH) and increased production of ROS (McCullough, et al., 2001). Glutathione has an important role in oxidative protein folding, assisting PDI, in the reduction of the disulphide bonds of misfolded proteins (Chakravarthi, et al., 2006). This evidence, taken together, suggest that cellular injury, such as from the acid exposure of GORD, a known precursor of BO, results in the accumulation of misfolded proteins in the ER, depleting cellular GSH and so leading to an increase in oxidative protein folding to compensate.

Western Blotting of lysates of the adenocarcinoma cell line OE33 compared to the squamous cell carcinoma cell line OE21 showed a greater sensitivity to stress, induced by deferoxamine mesylate (DFOM), $CoCl_2$ and Tunicamycin, determined by an increase in ERO1α expression in the OE33 cell line compared to OE21 cells (Baillie, et al., 2013). A natural consequence of the increase in expression of ERO1α would , therefore, be an increase in the generation of H_2O_2 (Figure 1.4A) as a by product. However, as can be seen in Figure 1.4 B and C both GPx7/8 and Prdx4, resident in the ER can utilise H_2O_2 to both remove ERO generated H_2O_2 and to increase protein folding. Ramming et al showed that loss of GPx8 resulted ER stress, leakage of H_2O_2 into the cytosol and cell death. They suggest that the ER resident GPx's, particularly GPx8, rather than Prdx4 are responsible for the

prevention of H_2O_2 accumulation and leakage from the ER and that Prdx4 only assists in H_2O_2 detoxification when levels of ERO catalysed H_2O_2 is maximised (Ramming, et al., 2015). Further Peng et al demonstrated that GPx7 has the capacity to prevent oxidative DNA damage. They showed that GPx7 expressing cells had lower levels of H_2O_2, intracellular ROS and oxidative DNA damage, in particular double strand breaks compared to controls when exposed to an acidified bile acid cocktail (Peng, et al., 2012). That the protective ability of GPx7 and Prdx4 does not seem to occur suggests that either the production of H_2O_2 overwhelms the ability of Gpx7/8 and Prdx4 or that something happens in normal squamous epithelium of the oesophagus that disrupts or reduces their ability to utilise and reduce H_2O_2 resulting in its accumulation and in turn oxidative DNA damage. Some evidence for loss of H_2O_2 protection currently exists with regards to GPx7. Peng et al demonstrated that the GPx7 promoter was silenced by location specific methylation *in vitro* and *in vivo* mouse models of OAC. They further demonstrated that re-expression of GPx7 in these models led to a reduction in tumour growth and an increase in cell senescence and suggest that GPx7 has a possible tumour suppressor role in OAC (Peng, et al., 2014). The loss of GPx7 has been thought to play a major role in the pathogenesis of BO, experiments have shown that loss of GPx7 can activate pro inflammatory pathways through activation of NF-κβ via TNF-α induction (Peng, et al., 2014). This finding correlates well with evidence that the bile salt deoxycholic acid imparts resistance to apoptosis via NF-κβ activation and induces ROS/RNS production and DNA damage, particularly double strand breaks in tissue biopsies from patients with benign BO (Huo, et al., 2011). Deoxycholic acid did not induce DNA damage or activate NF-κβ in normal intestinal cells (Zhang, et al., 2009) (Huo, et al., 2011), suggesting that while loss of GPx7 may have a role in

the pathogenic transformation of BO to OAC. Its role in the initial transformation of the oesophagus to BO is unclear.

In addition to evidence linking ERO1-α and the loss of GPx7 with BO and OAC, Prdx4 has also been linked with progression in many cancers, such as, breast and prostate carcinoma (Rafiei, et al., 2015), primary colon tumours (Leyssbill, et al., 2011), glioblastoma multiforme, an aggressive brain malignancy (Kim, et al., 2012) and oral cavity squamous cell carcinoma (Chang, et al., 2011). In particular Prdx4 seems important in the metastasis of these cancers (Chang, et al., 2011) (Rafiei, et al., 2015) and in the silencing of apoptotic pathways (Leyssbill, et al., 2011) (Wang, et al., 2009). In breast and prostate cancers, it has been observed, by mass spectrometry that peroxiredoxins were secreted from the cancer cells. A meta analysis of samples taken from breast and prostate cancer patients determined that the gene expression of Prdx4 was increased in carcinoma tissues. It was also seen that patients who developed metastasis had significantly increased expression levels of Prdx4 than those who remained metastasis free after 5 years. The bone is a common site of metastasis in breast and prostate cancers (Hess, et al., 2006) and in order to release bone-bound growth factors and aid invasive proliferation cancer cells must recruit terminally differentiated osteoclasts. Rafiei et al showed that secreted Prdx4 had the capacity to induce osteoclastogenesis and that cell lines deficient in Prdx4 demonstrated a decreased ability to stimulate osteoclast formation *in vitro*. Nude mice, tibial injected with PC3 cancer cells in which Prdx4 had been knocked down developed significantly smaller osteoclastic lesions and a decrease in osteoclast number compared to control PC3 cells (Rafiei, et al., 2015). A similar finding has also been found in oral cavity squamous cell carcinoma (OSCC) which is associated with a high probability of cervical lymph node metastasis. A proteomic

analysis by Chang et al, showed differential expression of Prdx6 when comparing metastatic and primary OSSC tumours. Analysis by immunohistochemistry revealed significantly (P <0.0001) higher levels of Prdx6 expression between tumour cells and neighbouring epithelial cells and in 31 metastatic lymph node tumours compared to corresponding primary tumours (Chang, et al., 2011). In glioblastoma multiformes (GBM),an aggressive brain malignancy, Kim et al found that Prdx6 expression was unregulated in humans and in mouse GBMs, relating Prdx6 expression with an increase in ROS. They detected an increase in ROS in mouse GBMs, compared to wild type controls suggesting that Prdx6 perhaps helped promote GBM growth. In order to test this hypothesis they used a lentiviral, GFP tagged expression system to knockdown Prdx6 expression in GBM neurospheres. This resulted in an increase in ROS accumulation, DNA damage, an increase in apoptotic cell number and a reduction in GBM growth (Kim, et al., 2012). This finding is supported by a small study in colon adenocarcinoma, where Prdx6 was also found to be over expressed in tumour cells compared to normal colon tissue. Here knockdown of Prdx6 gene expression resulted in an increase in apoptosis (Lyngdoh, et al., 2011). While this increase in apoptosis may be related to its antioxidant properties, there is evidence to suggest that over expression of Prdx6 may actually inhibit part of the apoptotic pathway by downregulating TNF-related apoptosis-inducing ligand (TRAIL) independent of ROS production (Wang, et al., 2009). Taken together this evidence suggests a significant role for Prdx6 in various diverse cancers, it is therefore not a great leap to imagine that disregulation of Prdx6 may have a role in OAC and therefore possibly in BO.

m

1.7 Anterior Gradient 2, an ER resident member of the PDI family which may have a role in the pathogenesis of Oesophageal Adenocarcinoma.

Anterior Gradient 2 (AGR2) is an ER resident member of the PDI super family (Persson, et al., 2005) it was first discovered in *Xenopus laevis* cement glands where it has a role in ectoderm patterning (Aberger, et al., 1998). In *Homo sapiens* AGR2 has a role in mucus production, particularly the MUC2 mucin in the intestine (Bergstrom, et al., 2014) (Park, et al., 2009) and the MUC1 and MUC5AC family members (Patel, et al., 2013). Like other ER proteins AGR2 contains a C-terminal localisation sequence (Figure 1.5), however rather than the usual KDEL, sequence (Munro & Pelham, 1987), AGR2 contains a novel KTEL sequence, Deletion of this motif results in AGR2 secretion and loss of AGR2 function (Gupta, et al., 2012). Various studies have shown that while AGR2 exists intracellularly it can also be secreted (Gupta, et al., 2012), which has important functions related to health and disease (Bergstrom, et al., 2014) (Fessart, et al., 2016). AGR2 contains a single thioredoxin fold domain, comprising of a CxxS motif rather than the classical CxxC motif (Figure 1.5), suggesting that AGR2 may be a late evolving member of the PDI family (Brychzva, et al., 2015) (Persson, et al., 2005). Recent evidence suggest that AGR2 may form dimers through the single cysteine of its CxxS motif suggesting that dimerisation may be required for disulphide exchange between AGR2 and its client proteins (Clarke, et al., 2014). Experiments by Ryu *et al* have shown both that AGR2 interacts with BiP/GRP78 and that dimerisation is required for the interaction (Ryu, et al., 2012) although what other client proteins AGR2 interacts with and by what mechanism AGR2 facilitates disulphide exchange, if it indeed does, is so far not clear.

m

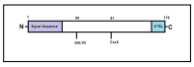

Figure 1.6: ADR2. Showing the Kex2 N-terminal signal sequence, the α-pair domination motif (green box), KTEL ER retention motif (blue box), and the Lys-K motif. [Gupta, et al., 2013] [Piya, et al., 2022] [Rizzi, et al., 2013] [Previato, et al., 2020]

Other than AGR2s role in disulphide bond formation and the trafficking of large cysteine rich glycoproteins, such as the mucin MUC2 (Park, et al., 2009) and MUC1 and MUC5AC (Patel, et al., 2013) little seems to be known about AGR2's role in normal physiology. Of more importance is the role that AGR2 also has in disease. AGR2 appears to have roles in a number of cancers, in particular hormone dependant breast and prostate cancer and in colorectal, pancreatic and gastric (hormone independent) cancers (Brychtova, et al., 2011). As an ER resident protein AGR2 has a role in the control of ER homeostasis and its expression is increased as part of the unfolded protein response to ER stress (Higa, et al., 2011). In cancer biology AGR2 seems to be involved in a number of processes relating to cell adhesion (Patel, et al., 2013) metastasis in oestrogen receptor positive breast cancer (Fletcher, et al., 2003) and as a survival factor (Pohler, et al., 2004). Although in breast and prostate cancer increased AGR2 expression seems to be related to hormonal stimulation (Ku, et al., 2013) there are several strong links that suggest that ER stress plays an important role in AGR2s involvement in cancer. Experiments by Dumartin *et al* showed that in pancreatic ductal adenocarcinoma (PDAC) increased AGR2 expression was present in the early stages of neoplastic transformation and as such preceded the development of PDAC. They found that discrete subpopulation of AGR2-expressing cells was present neighbouring pre-neoplastic lesions and that in primary cells from a patient-derived xenograph model, that AGR2 was overexpressed in cancer stem cells compared to cancer cells of non-stem origin. Further Dumartin *et al* saw, in a mouse model, that AGR2 induction preceded the development and formation of pre-neoplastic lesions and that deletion of AGR2 expression inhibited lesion growth. They also showed that tunicamycin induced ER stress increased the expression of AGR2 and that increased AGR2

m

expression in pancreatic intraepithelial neoplasia persisted after markers of the unfolded protein response were switched off (Dumartin, et al., 2016). How AGR2 expression is involved in neoplastic transformation is unclear although evidence suggests that AGR2 is secreted from that ER (Gupta, et al., 2012) and it is this secreted AGR2 that maybe responsible for driving transformation. Experiments by Fessart et al provide some evidence for this, in their study they showed that AGR2 was present within the extracellular matrix. Depletion of AGR2 from a lung carcinoma cell line resulted in a loss of tumourgenicity and metastatic potential and that the addition of recombinant human AGR2 to the media of several adenocarcinoma cell lines depleted of AGR2 restored their ability to form tumour organids. They also demonstrated the metastatic potential of AGR2. In vitro normal human bronchial epithelial cells (HBEC) form polarised, spherical organids with hollow lumens; addition of AGR2 to the extracellular matrix resulted in the formation of large non polarised, undifferentiated organids lacking a lumen. (Fessart, et al., 2016) suggesting a possible mechanism where, if normally ER localised AGR2, was secreted it may be able to induce tumourgenesis.

Finally a role for AGR2 has been suggested as a survival factor in cancer, particularly in GAC. A study by Pohler et al showed that AGR2 was overexpressed in lysates of BO tissue in comparison to normal oesophageal tissue lysates and that overexpression of AGR2 attenuated the phosphorylation of p53, a tumour suppressor protein in response to UV induced stress. However AGR2 does not seem to interact directly with p53, so the mechanism by which it suppresses p53 and p53 controlled apoptosis is as yet unclear (Pohler, et al., 2004). It is evident, nevertheless, that AGR2 appears to be heavily linked to the pathogenesis of a number of cancers via many different roles.

m

In summary, Barrett's Oesophagus is a complex disease, related to the fact that the cells of the oesophagus are under constant environmental pressures, from heat stress (due to hot food intake) from chemicals and food products and from exposure to refluxed acid, pepsin and bile products. This scenario is exacerbated further in those that suffer from GORD. Such a complex microenvironment may mean that the exact cause of the transition from BO to OAC is individual to each patient, however there are many possible targets for biomarker developments that may aid in determining the risk of those presenting with Barrett's Oesophagus transitioning to OAC.

1.8 Aims

There is evidence to suggest a link between the damage caused by ROS such as peroxide and oxygen radicals and BO. Cells and tissues have a system of antioxidant proteins and other molecules that prevent damage by ROS, including glutathione peroxidases (GPx) and peroxiredoxins (Prdx). Accumulation of ROS may favour the transition of BO to OAC. Recently, members of the GPx and Prdx families have been implicated in controlling protein folding and stress responses in the endoplasmic reticulum. However, the extent to which members of the GPx and Prdx families are dysregulated in BO and OAC is not known.

The aim of the is thesis is to

- Determine the expression levels of the GPx family member GPx7 and the Prdx4 in oesophageal cells.
- Expose the oesophageal cells to ER stress inducing stimuli and analyse the expression profiles of GPx7 and Prdx4
- To relate any findings to the whole organism the expression of GPx7 and Prdx4 in normal oesophageal will be compared with tissue taken from patients with BO and OAC and examined by immunohistochemistry using confocal microscopy.

Materials and Methods

2.1 Antibodies

The following antisera was used, monoclonal antiserum against Prdx6 [TA](16943) and GPx7 [2704](3727) were obtained from Abcam. A polyclonal GPx7 antiserum was a gift from the Yang Group (Wang, et al., 2014)Two antisera against Elp57 were used the first, Elp57 (G117) was obtained from Cell Signalling and the second was a gift from Neil Bulleid (Bulleid & Jessop, 2004). Polyclonal antiserum against CANX and CALR was a kind gift from the Okabe Group (Ikawa, et al., 2011). Polyclonal Antiserum against BIP (H-129), antiserum against Insulin (H-68: s-c9168) and ERO1-Lα (H-90:sc-66354) were obtained from Santa Cruz Biotechnologies. Monoclonal antiserum against AGR2 was obtained from Cell Signalling. Antiserum against PDI (MA3-019) was obtained from Bioreagents and Antiserum against PDIp was a kind gift from Michael Lam (Desilva, et al., 1997)

2.2 Cell Lines

The following commercial, immortalised cell lines were used HT1080 (L Breakman) a fibrosarcoma cell line, originally obtained from fibrosarcoma tissue taken by biopsy from a 35- year old human male (Rasheed S, 1974) , HeLa (NBuilded), derived from cervical cancer cells (Scherer W, 1953), OE19 (96071721, ecacc) was derived from an Adenocarinoma of Cardia taken from a 72 year old male, OE21 (96062201, ecacc) derived from a Squamous carcinoma taken from a 68 year old male and OE33 (96070808, ecacc) derived from an Adenocarcinmas in Barrett's taken from a 73 year old female (Rockett J, 1997).

2.3 Cell Culture

HT1080 cells were maintained in Dulbecco's modified Eagle's medium (DMEM Gibco Thermofisher Scientific), Hela cells were maintained in Minimum Essential Medium (MEM, Gibco Thermofisher Scientific) and OE19 and OE33 cells were maintained in Roswell Park Memorial Institute Medium (RPMI 1640 L-glutamine, Gibco Thermofisher Scientific) all supplemented with 8% Fetal Bovine Serum (FBS, Sigma) 2mM glutamax (Invitrogen) 100 units/ml penicillin and 100 units/ml streptomycin (Invitrogen) at 37°C and 5% CO_2. All cell lines were serially passaged at 70-80% confluency using 0.05% trypsin (Trypsin-EDTA, Invitrogen) to digest the monolayer, before resuspending in fresh media Hela and HT1080 cells were typically split 1:10 into T75 flasks (TPP Helena Biosciences) and the OE cell lines were diluted 2:5 into T25 flasks (TPP Helena Biosciences). All cell cultures were kept in an incubator (Binder) in humid conditions in 5% CO_2 (low pressure) at 37°C.

2.4 Transfection

GPx7(Myc-DDK tagged) cDNA (Origene) and the ERO1-α mutant cDNA C394A (created by site directed mutagenesis by Dr Adam Benham (Benham, et al., 2000) using a Stratagene quick change kit) were used for the transfection of HeLa cells. The HeLa cells were cultured, in 6cm culture dishes, containing 3 13mm coverslips, to 80% confluence in Minimum Essential Medium (MEM, Gibco Thermofisher Scientific). The cells were transfected using Lipofectamine 3000 (Invitrogen, Thermofisher). A master mix was prepared for each cDNA to be transfected, For the Gpx7 master mix 2µg Gpx7 cDNA and 4µl p3000 were added to 125µl Opti-MEM (Gibco Thermofisher Scientific) and for the ERO1-α mutant cDNA C394A master mix

1µg of C3HA cDNA and 4µl p3000 were added to 125µl Opti-MEM. The transfection reagent was prepared in eppendorf tubes each containing 125µl Opti-MEM and 7.5µl Lipofectamine 3000 and an equal amount of each cDNA master mix was then added to each tube which were then left for 5 minutes to incubate before adding to the 80% confluent HeLa cells, which were washed twice with 1ml sterile PBS before the transfection reagents were added. Each dish was then left to incubate, at 37°C, 5% CO_2, for 2 hours after which 1ml of MEM was then added to each dish, then left overnight to reach full confluence before analysing by immunofluoresence..

2.5 Cell Lysate Generation

Cells were lysed in lysis buffer (1 mM phosphate buffered saline (PBS, Sigma) with 1% Triton X-100 (Sigma), supplemented with 10 µg/ml each of chymostatin, leupeptin, antipain and pepstatin A (CLAP) and 20mM N-ethylmaleimide (NEM) when required. Nuclei were removed by centrifugation at 16,100g (Eppendorf) for 10 minutes at 4°C, and the Post-nuclear supernatant collected, flash frozen in liquid Nitrogen and stored at -20°C until analysed by SDS-PAGE

2.6 Cell Lysate Protein Quantification

A Pierce™ BCA Protein Assay Kit (Thermo Scientific) was used to determine the protein concentration. The assay kit is a colorimetric detection assay based on the biuret reaction, the reduction of Cu^{2+} to Cu^{+}, with detection and quantification of total protein utilising a reagent containing bicinchoninic acid (BCA). This produces a

purple coloured reaction product formed by the chelation of two molecules of BCA to one cuprous ion. This is emits a strong absorbance at 562nm that is nearly linear over a protein concentration range of 20-2000µg/mL. BSA standards from 25µg/mL and 2000µg/ml diluted in lysis buffer (minus CLAP and with or without NEM, sample dependant) were prepared in order to generate a standard curve. Then 0.05mL of the lysate and each standard were combined with 1mL of the Kit's working reagent in separate tubes (Eppendorf) and incubated, in a water bath, at 37°C for 30 minutes, the tubes were then cooled to room temperature and read on a spectrophotometer(Eppendorf Bio Photometer) at 562nm. All samples were read within 10 minutes as the BCA assay has no true endpoint and so the colour will develop further over time. The standard curve was drawn and lysate concentration determined using Microsoft Excel.

2.7 Immunoprecipitation

Protein A sepharose beads (Sigma) were prepared by diluting 1:10 of bead slurry in lysis buffer. The beads were spun at 1500g, 5 minutes, 4°C in lysis buffer (without NEM or CLAP). Then the supernatant was aspirated off and the beads were resuspended in fresh lysis buffer and spun again at 1500g, 5 minutes, 4°C. The supernatant was discarded and the cells were resuspended in 6ul of antibody in lysis buffer and incubated for 2 hours at 4°C with rocking. After incubation the beads were spun at 1500g, 5 minutes, 4°C, discarding supernatant, resuspended in lysis buffer, then spun again at 1500g, 5 minutes, 4°C. The supernatant was discarded and the beads were then resuspended in a 1:4 dilution of cell lysate in lysis buffer, then incubated for 1 hour at 4°C with rocking. The bead cell mixture was then spun

m

twice at 1500g, 5 minutes, 4°C, discarding supernatant and resuspending in fresh lysis buffer between spins. Finally the supernatant was aspirated off and the bead cell mix was resuspended in 50mM DTT in 2x laemmli sample buffer (NuPage LDS sample buffer, Invitrogen), heated at 95°C for 5mins, then analysed by SDS-PAGE (section 2.10) .

2.8 Treatments

In order to observe if any change in protein expression was redox dependant or independent, OE19 cells were treated with either under reducing or oxidising conditions. To examine the effects of reducing conditions on protein expression OE19 cells were cultured in three 6cm dishes to confluence. The first dish was kept as a control, the culture media was aspirated off and fresh RPMI was added and the cells were incubated, at 37°C 5% CO_2, for 5 minutes. The cells were then washed once for 5 minutes with PBS with 20mM NEM, then washed once more for 5 minutes with just PBS before being lysed. For dish two the media was aspirated and RPMI supplemented with 5mM DTT was added, the cells were then incubated for 5 minutes then washed, once for 5 minutes with PBS with 20mM NEM, then washed once more with just PBS for 5 minutes before being lysed. The final dish was aspirated and RPMI supplemented with 5mM DTT was added, the cells were then incubated for 5 minutes. The supplemented media was aspirated off and fresh, unsupplemented RPMI was added and the cells were incubated for a further 10 minutes before being washed, once for 5 minutes with PBS with 20mM NEM, then washed once more with just PBS for 5 minutes before being lysed.

To examine the effects of oxidising conditions on protein expression OE19 cells were cultured in three 6cm dishes per cell line to confluence. The first dish was kept as a

control, the culture media was aspirated off and fresh RPMI was added and the cells were incubated, at 37°C 5% CO_2 for 5 minutes. The cells were then washed once for 5 minutes with PBS with 20mM NEM, then washed once more for 5 minutes with just PBS before being lysed. For dish two the media was aspirated and RPMI supplemented with 5mM Diamine was added, the cells were then incubated for 5 minutes then washed, once for 5 minutes with PBS with 20mM NEM, then washed once more with just PBS for 5 minutes before being lysed. The final dish was aspirated and RPMI supplemented with 5mM Diamine was added, the cells were then incubated for 5 minutes. The supplemented media was aspirated off and fresh, unsupplemented RPMI was added and the cells were incubated for a further 10 minutes before being washed, once for 5 minutes with PBS with 20mM NEM, then washed once more with just PBS for 5 minutes before being lysed.

2.9 Immunofluorescence

2.9.1 Standard Protocol

A 24 well plate was prepared by the addition of a 13mm glass coverslip to each well to be used. The wells were then washed with 500µl PBS. Cells were culture to 70-80% confluency then detached using 0.05% trypsin (Trypsin-EDTA, Invitrogen), diluted 1 in 10 with the appropriate media. 500µl of cell suspension was added to each well containing a coverslip and then incubated overnight at 37°C, 5% CO_2 to allow the cells to adhere to the coverslips

The media was removed and discarded and the coverslips were washed twice with 500µl PBS++ (PBS containing 1mM $MgCl_2$ and 0.5mM $CaCl_2$). The cells were then fixed in 500µl 4% Paraformaldehyde (diluted from 16% stock in dH2O) for 10 minutes. The cells were then washed twice with 500µl PBS++ before free aldehyde

groups were the quenched in 500µl 50mM NH4Cl for 10 minutes then washed three more times in 500µl PBS++. The cells were permeabilised in 500µl 0.1% Triton X-100 in PBS++ for exactly 10 minutes, then washed in 500µl PBS++ for 5 minutes. then blocked by washing in twice in 500µl BSA (Sigma) in PBS++.

The blocking solution was fully removed and either 20µl Control (0.2% BSA in PBS++) or 20µl of the appropriate primary antibody or a mix of primary antibodies from two different host animal species, diluted in PBS++ according to Table 2.1, was added to each coverslip, the plate was then covered and the cells incubated at room temperature for 30 minutes, washed three times 5 minutes with 500µl PBS++ before incubating in 20µl of the appropriate secondary antibody (Table 2.1), diluted 1:1000 in PBS++ for 20 minutes in a dark drawer.

The coverslips were then washed twice times 5 minutes in 500µl 0.2% PBS++, once for 5 minutes in 500µl PBS++ and then for 5 minutes in 40µl 1:1000 DAPI in PBS++ all in the dark. The coverslips were washed a final time in dH$_2$O, to prevent salt build up before each coverslip was removed and mounted, cell side down, onto a labelled microscope slide using hard set Vectrashield. The slides were left , covered on the bench for 20 minutes then transferred to 4^{o}C till set before being examined on a Zeiss Apatome microscope.

2.9.2 Immunofluorescence of AGR2 with Methanol Permeabilisation

A 24 well plate was prepared by the addition of a 13mm glass coverslip to each well to be used. the wells were then washed with 500µl PBS. Cells were culture to 70-80% confluency then detached using 0.05% trypsin (Trypsin-EDTA, Invitrogen), diluted 1 in 10 with the appropriate media. 500µl of cell suspension was added to

each well containing a coverslip and then incubated overnight at 37^{0}C, 5% CO_2 to allow the cells to adhere to the coverslips

The media was removed and discarded and the coverslips were washed twice with 500µl PBS++ (PBS containing 1mM $MgCl_2$and 0.5mM $CaCl_2$). The cells were then fixed in 500µl 4% Paraformaldehyde (diluted from 16% stock in dH_2O) for 10 minutes, then washed three times with 500µl PBS++. The coverslips were then covered with 500µl ice-cold Methanol and incubated at -20^{0}C for 10 minutes, the coverslips were then rinsed once in 500µl PBS++ for 5 minutes.

The cells were then blocked for 1 hour in 500µl Blocking buffer(5% normal goat serum, 0.3% Triton X-100 in PBS++). The blocking buffer was aspirated off then 20µl AGR2 antibody, diluted, according to Table 2.1, in 1%BSA, 0.3% Triton X-100 in PBS++) was added to each coverslip and incubated overnight at 4^{0}C. After primary antibody incubation the coverslips were washed three times for 5 minutes in PBS++ before incubating in 20µl of the appropriate secondary antibody(Table 2.1), diluted 1:1000 in PBS++ for 20 minutes in a dark drawer.

The coverslips were then washed twice times 5 minutes in 500µl 0.3% PBS++, once for 5 minutes in 500µl PBS++ and then for 5 minutes in 40µl 1:1000 DAPI in PBS++ all in the dark. The coverslips were washed a final time in dH2O, to prevent salt build up before each coverslip was removed and mounted, cell side down, onto a labelled microscope slide using hard set Vectrashield. The slides were left , covered on the bench for 20 minutes then transferred to 4^{0}C till set before being examined on a Zeiss Apatome microscope.

Primary Antibody	Host Species	Dilution	Secondary
Prdx4	Mouse	1:200	Alexa fluor 488
GPx7	Rabbit	1:200	Alexa fluor 594
GPx7	Mouse	1:200	Alexa fluor 488
ero1l	Rabbit	1:200	Alexa fluor 594
PDI	Rabbit	1:200	Alexa fluor 594
PDI	Mouse	1:200	Alexa fluor 488
CANX	Rabbit	1:500	Alexa fluor 594
CALR	Rabbit	1:500	Alexa fluor 594
AGR2	Rabbit	1:200	Alexa fluor 594

Table 2.1 A List of Primary antibodies u sed in immunofluorescence, showing host species, dilution and appropriate secondary Alexa fluor (Thermoscientific).

2.10 SDS-PAGE

Post-nuclear supernatants and immunoprecipitates were taken up in 2x laemmli sample buffer (NuPage LDS sample buffer, invitrogen), heated at 95^{0}C for 5mins, then analysed by SDS-PAGE.

Samples were run on an acrylamide gel containing SDS which comprised of a resolving gel and a stacking gel. The resolving gel comprised of either 10% or 12% Acrylamide (Severn Biotech), percentage dependant on the molecular weight of the protein under investigation, 375 M Tris (pH 8.8), 0.1% SDS (Sigma), 0.1% APS (Sigma) and 0.04% TEMED (Sigma). The resolving gel was cast in a Hoefer gel caster system, until polymerised fully, the running gel was covered with dH$_2$O to

ensure that the interface between the running gel and the stacking gel was smooth. Once polymerised the dH_2O was removed and the stacking gel was added, along with a 10 or 15 well comb. The stacking gel was comprised of 5% Acrylamide (Severn Biotech), 0.125 M Tris (pH6.8), 0.1% SDS (Sigma), 0.075% APS (Sigma) and 0.075% TEMED (Sigma). After the stacking gel had polymerised the gel was transferred to a mighty small II mini vertical electrophoresis unit and sufficient 1 x TGS electrophoresis running buffer (10x TGS running buffer (Biorad) diluted with dH_2O) to cover the gel. The comb was removed and samples were loaded alongside 5 µl of a known molecular weight protein marker (Biorad) All samples were equalised to 10µg/ml of protein per well and analysed under either non-reducing conditions or reducing conditions, with the addition of 50mM DTT to the sample buffer and ran at 50mA until the dye front reached the bottom of the gel, without running off, then the gel was either Western Blotted or Stained with Coomassie Blue.

2.11 Gel Staining

The gel was fixed in 50ml of fixing solution (7% Acetic Acid, 40% Methanol in dH_2O) for 10 minutes. The solution was removed and the gel was covered in Coomassie stain (20% Methanol and 80% Brilliant blue G-colloidal concentrate (Thermofisher)). The gel was left to stain overnight at room temperature on a rocker, then removed and destained with 50ml of destain solution (25% Methanol, 10% Acetic Acid in dH_2O) for 10 minutes, before removing and destaining, a second time, with 50ml 25% Methanol in dH_2O, overnight, whilst rocking. The destain was then removed and the gel was washed in dH_2O and then imaged on a gel documentation system.

2.12 Western Blotting

Protein's separated by SDS-PAGE were transferred from gel onto a PVDF membrane (Millipore) in transfer buffer (25 mM Tris-Base, 190 mM Glycine in 20% methanol), at 150 mA for 2hrs or overnight, at 4°C, at 30V. Prior to use in transfer the PVDF membrane was primed in methanol for 20 seconds. Membranes were then blocked 5% milk dissolved in TBS-T(10 mM Tris-base, 70 mM NaCl, 1.3M mM KCl, 0.1% Tween-20, PH 9-9.4) either overnight at 4°C or 1hr at room temperature, with rocking. Membranes were then washed three times, for 5 minutes each, with TBS-T, before being incubated in the primary antibody, in 5% milk/TBS-T either overnight, at 4°C or for 1hr, with rocking. Table 2.2 lists the primary antibodies used, their host species and corresponding dilutions. Membranes were rinsed in TBS-T, then washed 4 times, for 5 minutes each, in TBS-T, after which, the membranes were incubated with a secondary antibody (DAKO) corresponding to the host animal species, see Table 2.2, diluted 1:2000 in 5% milk/TBS-T for 1hr, rinsed in TBS-T, then washed 4 times, for 5 minutes each, in TBS-T then once, for 5 minutes, in TBS. 500µL ECL (Amersham) was then added to the membrane before it was exposed to film (Thermofisher) then developed in an x-ray developer (XOMAT).

Primary Antibody	Host Species	Secondary	Dilution
Prdx4	Mouse	GAMPO	1:1000
GPx7	Rabbit	SARPO	1:1000
GPx7	Mouse	GAMPO	1:1000
ERp27	Rabbit	SARPO	1:1000
PDI	Rabbit	SARPO	1:1000
CANX	Rabbit	SARPO	1:1000
CALR	Rabbit	SARPO	1:1000
AGR2	Rabbit	SARPO	1:1000

Table 2.2 A list of primary antibodies used in Western Blotting, including host animal species, appropriate secondary and antibody dilution used.

2.13 Molecular Biology

2.13.1 Transformation of DH5α cells

DH5α competent cells were transfected with mouse GPx7[Myc-DDK tagged, in pCMV6, Figure 2.1) cDNA (Origene) for mini prep. For each transformation 1µl GPx7 cDNA (2µg) was heat shocked at 42^{0}C for 1 minute, added to 50µL of DH5α competent cells, then incubated at 42^{0}C for another minute. LB broth (Fisher, 10g Tryptone, 5g Yeast extract, 10g NaCl made up to 1l pH7.0) was then added for a total final volume of 1ml and incubated at 37^{0}C for 45 minutes then centrifuged at 12000 rpm for 1 minute. Supernatant was removed and the cell pellet was re-suspended in 100µl of LB broth supplemented with0.25mg/ml Kanamycin and spread on LB-agar (Fisher) plates, supplemented with0.25mg/ml Kanamycin, overnight at 37^{0}C. Single colonies were picked and inoculated, overnight at 37^{0}C, with constant agitation, into 5ml of LB broth supplemented with 0.25mg/ml

Kanamycin then used to extract plasmid DNA using a Qiagen Mini Prep kit, according to the manufacturer's instructions.

Figure 2.1 Open Reading Frame (ORF) Nucleotide sequence for Mouse OPeT. Myc-DDK-tagged at the C-terminus of the protein, in pCMV6 (OriGene MR203.TA0) Heis-Cloning site Blue-ORF Green-Tag(s)

Bacterial cells were harvested by centrifugation at 5400g for 10 minutes at 4^{0}C and the cell pellet was then re-suspended in 250µl of Buffer(P1 with added Rnase A), in a 1.5ml microcentrifuge tube. 250µl of Buffer(P2) was then added and mixed by inversion 6 times until the solution became viscous and slightly clear. Then 350µl Buffer(N3) was added and the solution mixed, by inversion, until it became colourless. The solution was then centrifuged at 17,900g for 10 minutes, the supernatant was collected, by pipetting, into a QIAprep spin column and spun at 17,900g for 60 seconds, discarding the flow through. The spin column was washed with 0.75ml of Buffer (PE) and spun at 17,900g for 60 seconds, discarding the flow through after which it was spun for a further 60 seconds to remove residual wash buffer. DNA was eluted into a clean 1.5ml microcentrifuge tube, by the addition of 50µl of Buffer(EB, 10mM Tris-Cl, pH-8.5) to the centre of each spin column, the

column was placed in the microcentrifuge tube then left to stand for 60 seconds and then spun at 17,000g for 60 seconds. DNA concentration was determined on a Labtech Nano-drop spectrophotometer.

2.13.3 Gel Electrophoresis

Agarose Gel Electrophoresis was used to identify the presence of GPx7 DNA in samples from Mini Prep. A 1% agarose gel was used to run the DNA samples, the gel was made from 1.2g Agarose (Invitrogen), 5.1µl ethidium bromide (Fisher) and 120ml 0.5x TAE buffer, diluted from a sterile 50x stock solution (60.5g tris base, 14.3ml glacial acetic acid, 25 µl 0.5M EDTA made up to 250ml with dH_2O), each lane was loaded with 10µl of sample containing either 1µl 1kb Ladder (Bioline, HyperLadder™1kb) and 9µl DNAse free H_2O, 1µl mini prep sample, 1µl loading buffer and 8µl DNase free H_2O or a reference sample of 1µl Gpx7 cDNA, 1µl loading buffer and 8µl DNase free H_2O. The gel was submerged in TAE buffer and the samples were run at 100v for 30 minutes before visualising under UV.

2.14 Tissues

Human Pancreatic Tissue was obtained from Medical Solutions PLC. Normal Oesophagus, Gastric, Barrett's Oesophagus and Oesophageal-Gastric Junction Tumour Tissue was provided by material transfer agreement from the Department of Histology at James Cook University Hospital.

2.15 Immunohistochemistry of human tissue sections

Paraffin embedded tissue was cut to 4um sections using a microtome, the section 'ribbons' were floated in a 37°C water bath for a few minutes only, then floated sections were lifted out of the water using polylysine coated slides and left to dry overnight on a 40°C heat bed.

2.15.1 Initial Staining Method

The slides were incubated at 50°C overnight prior to staining then loaded into a Thermo Scientific Sequenza Manual Staining Rack. Each section was washed sequentially with 120µl the following washes, 7 minute wash in Histoclear (Agar Scientific), a second 7 minute wash in Histoclear, a 7 minute wash in 100% ethanol, a 5 minute wash in 95% ethanol, a 5 minute wash in 70% ethanol and finally a 3 minute wash in tap water. Each section was washed for 15 minute in 3% H_2O_2 in methanol to block endogenous peroxidase activity.

Slides were then transferred to a rack for antigen recovery and incubated in 10mM sodium citrate buffer (pH 6.0) for 20 minutes in a 90°C waterbath, then cooled down on ice to room temperature. Sections were ringed with a hydrophobic pen (Imm Edge Pen, Vector Laboratories H-4000) and 100ul 0.2% BSA in PBS was added to each section for 5 minute. Sections were then blocked, for 30 minutes, in 100µl 0.2% PBS plus 5% Normal Goat Serum (DAKO) then incubated for 1 hr with 100µl primary antibody:antibody (antibodies used were the same as those listed in Tables 2.1 and 2.2) diluted in 0.2% PBS plus 5% Normal Goat Serum. Sections were then washed for 5 minutes with 100µl 0.2% BSA in PBS before incubation for 45 minutes with 100µl 1% Reagent C (DAKO kit K0493) in PBS. Reagent C solution was removed

57

by tipping the slide and blotting the edge of each ringed section with tissue then washed for 5 minutes with 100µl 0.2% BSA in PBS then incubated for 30 minutes with 100µl 1% Reagent A + 1% Reagent B in PBS, prepared 15 minutes prior to incubation (DAKO, K4004D), then washed for 5 minutes in PBS. DAB solution was prepared by dissolving fully 1 H2O2 tablet and 1 DAB tablet (both Sigma) in 5ml PBS) then 100µl of DAB-peroxide solution was added to each slide and left for 4 minutes, in the dark for 4 minutes, then rinsed in tap water. Slides were transferred to a slide rack and immersed in Harris Haematoxylin (Sigma) for 4 minutes, then transferred to tap water for 5 minutes. The slides were then transferred back to the Sequenza Staining rack. The sections were rinsed in 2 fast washes of 120µl 1% Conc HCL in Methanol. Then washed twice in 1min washes using 120µl tap water. The sections were the washed sequentially with the following washes: a fast wash twice in 120µl 70% ethanol, fast washed twice in 120µl 95% ethanol, washed for 5 minutes in 120µl 100% ethanol, then washed twice for 7 minutes in 120µl Histoclear. The sections were then mounted in DPX mounting medium and left to dry before examination under a Nikon microscope with a lens mounted Euromex CMEX 5mp wireless camera.

2.15.2 Adapted Staining Method

The slides were incubated at 50°C overnight prior to staining then loaded into a Thermo Scientific Sequenza Manual Staining Rack. Each section was washed sequentially with 120µl the following washes, 7 minute wash in Histoclear (Agar Scientific), a second 7 minute wash in Histoclear, a 7 minute wash in 100% ethanol, a 5 minute wash in 95% ethanol, a 5 minute wash in 70% ethanol and finally a 3

minute wash in tap water. Each section was washed for 15 minute in 3% H_2O_2 in methanol to block endogenous peroxidase activity.

Slides were then transferred to a rack for antigen recovery and incubated in 10mM sodium citrate buffer (pH 6.0) for 20 minutes in a 90°C waterbath, then cooled down on ice to room temperature. Sections were ringed with a hydrophobic pen (Imm Edge Pen, Vector Laboratories H-4000) and 100ul 0.2% BSA in PBS was added to each section for 5 minute. Sections were then stained using the Vector Laboratories RTU Vectastain universal Quick kit (PK-7800). The sections were transferred to a moist chamber and blocked in 100µl prediluted blocking serum (2.5% Normal Horse Serum for 10 minutes, excess serum was then blotted from sections which were then washed for 5 minutes in 100µl PBS. Sections were incubated in 100µl of the appropriate primary antibody (antibodies used were the same as those listed in Tables 2.1 and 2.2), diluted 1:200 in 0.2% BSA in PBS containing 1.5% prediluted blocking serum for 1hr. The sections were then washed for 5 minutes in 100µl PBS. Following this the sections were then incubated in one drop (~30µl) of prediluted biotinylated pan-specific secondary antibody for 10 minutes before washing for 5 minutes in 100µl PBS and then incubated in one drop of RTU streptavidinhrpetxidase complex reagent for 5 minutes. Sections were washed for 5 minutes in 100µl PBS and were incubated in 100ul of ImmPACT DAB peroxidase substrate (Vector Laboratories SK-4105 consisting of 30ul ImmPACT DAB chromogen in 1ml ImmPACT diluent) for 4 minutes in dark or until desired intensity developed then rinsed in 100µl tap water. Slides were transferred to a slide rack and immersed in Harris Haematoxylin (Sigma) for 4 minutes, then transferred to tap water for 5 minutes. The slides were then transferred back to the Sequenza Staining rack. The sections were rinsed in 2 fast washes of 120µl 1% Conc HCL in 70%

ethanol, then washed twice in 1 min washes using 120 µl Scott's tap water substitute (61.67 mM $NaHCO_3$, 166.16 mM $MgSO_4$ and rinsed in 120 µl dH_2O. The sections were then washed sequentially with the following washes a fast wash twice in 120 µl 75% ethanol, fast washed twice in 120 µl 95% ethanol, washed for 5 minutes in 120 µl 100% ethanol, then washed twice for 7 minutes in 120 µl Histoclear. The sections were then mounted in DPX mounting medium and left to dry before examination under a Nikon microscope with a lens mounted Euromex CMEX 5mp wireless camera.

Antibody Testing and Method Evaluation

3.1 Introduction

Immunohistochemistry (IHC) is the combination of anatomical, immunological and biochemical techniques to identify specific tissue components using the interaction of target antigens (tissue proteins) with an appropriately tagged antibody. Before embarking on the staining of the human patient samples, which were kindly provided by James Cook University Hospital, it was important to validate the IHC method to ensure the best consistency of results. In principle the IHC method consists of a number of discrete steps including sample preparation, tissue permeabilisation and antigen retrieval, staining, mounting and finally visualisation. In order to optimise these stages a series of experiments using commercially available pancreatic tissue was conducted before work using on the limited patient samples.

In addition, some antibodies, including those raised against calnexin (CANX) and calreticulin (CALR), which had been provided as gifts from the Okabe group (see Chapter 2.1), had not been tested on human tissues and their efficacy in immunohistochemistry, immunofluorescence and Western blotting (of human cell lines) had yet to be validated

3.1.1 Histology of the Pancreas

The majority of the human pancreas consists of exocrine tissue, arranged in lobules comprised of pancreatic acinar cells and ductal tissue which drains from the main pancreatic duct into the common bile duct (Keshav, 2004). Pancreatic acinar cells have a broad base with a narrow apical surface covered with a few short microvilli. The role of the acinar cells, of the exocrine pancreas, is in the production and

secretion of the precursors of a wide range of enzymes. As such the cells are rich in rER located primarily in the basal half of the cell. In contrast the apical half of the cell can contain a variable number of eosinophilic zymogen granules containing pre-synthesised enzymes depending on where the cell is in its secretory cycle (Stevens & Lowe, 1997).

In addition to the exocrine pancreatic tissue the pancreas also contains endocrine tissue situated in discrete islets throughout the main exocrine tissue, known as the Islets of Langerhans. The Islets of Langerhans are composed of many cell types including β cells, which secrete insulin, α cells which secrete glucagon and D cells which secrete somatostatin, the islets do not connect to the pancreatic ductal system but instead secrete directly into the bloodstream via an extensive capillary network of blood vessels (Keshav, 2004).

3.1.2 The role of the Calnexin and Calreticulin in the Endoplasmic reticulum.

Calnexin (CANX) and calreticulin (CALR) are ER resident chaperones, part of the lectin family of proteins. Along with ERp57, a thiol-disulphide oxidoreductase and member of the P2I family (Ellgaard & Frickel, 203), CANX and CALR interact with and aid in protein folding and disulphide bond formation of newly synthesised N-linked monoglycosylated glycoproteins that have undergone partial trimming of the core glycan ($Glc_3Man_9GlcNAc_2$) which is added at the N-terminus of nascent polypeptide chains at a side chain containing an Asparagine-X-Serine/Theonine sequence during translocation into the ER (Helenius, et al., 1997) (Ellgaard & Frickel, 203). CANX is a 65 kDa monoglycosylated type 1 membrane protein containing 573aa, which has its substrate binding domain located at the luminal side of the ER. In contrast its homologue CALR is a 46 KDa soluble protein of 400aa.

CALR has a KDEL ER retrieval sequence and a C-terminal region with a high negative charge, thought to be responsible for ER retention and Ca^{2+} binding. (Helenius, et al., 1997).

As has been briefly discussed in the introduction, ER resident chaperones and components of the oxidative protein folding machinery may have some link in the progression of Barrett's Oesophagus (BO) to Oesophageal Adenocarcinoma (OAC). While there is no evidence to suggest that ERp57, CANX and/or CALR are involved in OAC there are suggested links that involve ERp57 and CANX in other cancers. Dissemond et al demonstrated that, in human metastatic melanoma, there was a differential down regulation when comparing CANX and CALR. They found that CANX but not CALR was down regulated in melanoma metastsis, although they also observed that this downregulation, while being statistically significant was not absolute, in that it was only observed in approximately half of the melanoma cells (Dissemond, et al., 2004). In contrast up regulation of CALR expression has been found in invasive ductal breast carcinoma (Kabbage, et al., 2013) (Zamanian, et al., 2016) where it has been suggested that its up regulation may have an effect on the MAPK and p53 pathways (Zamanian, et al., 2016). Finally there is also a suggestion that partial or total loss of ERp57 by hypermethylation of its promoter in esophageal squamous cell carcinoma (ESCC) may contribute to tumourgenesis (Sheyhidin, et al., 2014). This evidence, taken together, suggested that it was worthwhile to test the efficacy of the CANX and CALR antibodies, in range of techniques to be used prior to commencement of the main body of experiments.

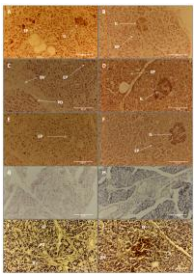

Figure 3.1. Initial Human Pancreatic Tissue Staining. (BP) Bovine pancreas (IL) Islets of Langerhans (D) Ductal tissue (A) Acinar tissue (BV) Blood vessel (H) Haematoxylin counterstain x10. (A) and **(B)** Human pancreas stained with rabbit polyclonal anti-insulin primary antibody and counterstained with haematoxylin. **(C)** Human pancreas control, 5 minutes DAB development **(D)** Human pancreas stained against insulin with 5 minutes DAB development. **(E)** Human pancreas control, 7 minutes DAB development **(F)** Human pancreas stained against insulin with 7 minutes DAB development. **(G)** Pancreas section stained with haematoxylin staining, Bluing, tap water **(H)** Pancreas section stained with haematoxylin staining, Bluing with Scott's water Substitute **(I)** Pancreas section staining control with 5 minutes DAB development and Scott's water bluing. **(J)** Pancreas section NBI staining with 5 minutes DAB development and Scott's water bluing.

3.2 Results

3.2.1Initial tissue staining experiments and method evaluations.

Initial staining of pancreas was carried out using commercially sourced pancreatic tissue stained with the anti insulin H86 antibody as an islet of Langerhans marker and a measure of success, using procedures optimised by Gunasekara et al (Gunasekara, 2006). As can be seen in Figure 3.1 A and B the DAB staining was strongest in the islets of Langerhans, as expected, but was also visible more weakly throughout the tissue. Because some background was visible around the islets of Langerhans further experiments were carried out varying the DAB development time. For the second set of experiments the DAB incubation time was increased from 4 minutes to 5 minutes (Figure 3.1C and D) and 7 minutes (Figure 3.1E and F) respectively and the H86 antibody (Figures 3.1D and F) was included alongside a negative control (Figures 3.1C and E). There was little difference in the intensity of the DAB staining between the 5 minute DAB developed, H86 stained, pancreatic tissue (Figure 3.1D) and the 7 minute DAB developed, H86 stained, pancreatic tissue (Figure 3.1F). However there appeared, in the control tissues (Figures 3.1C and E), a loss of the faint blueing from the Haematoxylin counterstain. Based on these observations it was therefore decided that a time of 5 minutes was about optimum for DAB development, although with the caveat that this result was only demonstrated using the anti insulin H86 antibody on human pancreatic tissue and may prove to be primary or secondary antibody dependant and/or tissue specific.

Of additional note in Figure 3 was the apparent lack of any visible counterstain from the Harris Haematoxylin used (see Chapter 2, 2.15.1). Since the blue nuclear stain from haematoxylin is pH dependant, its intensity could be increased by substituting

Scott's Tap Water Solution in place of normal tap water (Brown, 2002). To test this pancreatic tissue was stained with haematoxylin then rinsed in either tap water (Figure 3.1G) or a solution of Scott's tap water (Figure 3.1H). From this experiment it was apparent that Scott's tap water gave a better staining result and so this was then further utilised when co-staining with DAB. Pancreatic tissue was then stained with the N66 antibody, as a positive control (Figure 3.1I) or without H66 (Figure 3.1J) as a negative control and compared. As can be seen in Figure 3 (I) and J) the use of Scott's tap water gave much better contrast than those previously stained with tap water (Figures 3.1A-F).

3.2.2. CALR is expressed strongly in all cell lines and exhibits a staining pattern which suggests that it is predominantly ER localised

Polyclonal antibodies raised, in Rabbit, against CALR and CANX (see Chapter, 2 section 2.1) were tested in immunofluorescence. CALR is an ER localised protein, so in order to validate the specificity of CALR in immunofluorescence the cell line HT1080 was incubated with CALR as per the standard protocol (see Chapter 2, section 2.9.1). Additionally three different CALR antibody dilutions were titrated against a 1:200 dilution of PDI as a positive control

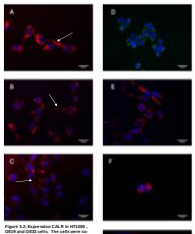

Figure 3.2: Expression CALR in HT1080 , OE33 and OE33 cells. The cells were co-stained with DAPI (nucleus, blue) and imaged at x63 magnification with an oil immersion objective and a numerical aperture 35µm. (A-C) HT1080 cell line stained with different dilutions of the CALR antibody (n=3) **(A)** 1:200 dilution (n=3) **(B)** 1:500 dilution (n=3) and **(C)** 1:1000 dilution (n=2). secondary Alexa fluor 488 **(D)** HT1080 cell line stained with 1:500 CALR dilution (n=2). secondary Alexa fluor 488 **(E)** OE21 cell line stained with 1:500 CALR dilution (n=2) . secondary Alexa fluor 594 **(F)** OE33 cell line stained with 1:500 CALR dilution (n=2) . secondary Alexa fluor 594 **(G)** HT1080 cell line stained with 1:200 PDI dilution (n=2) . secondary Alexa fluor 564. Arrows indicate staining which maybe cytoplasmic

and co-stained with DAPI, as a marker of the nucleus (Figure 3.2 A-C and G). PDI shows the classical staining attributed to the ER in Figure 3.2G surrounding the DAPI stained nucleus, stained in blue with the PDI localised in the ER seen primarily to one side of the cell. Given that the ER is a continuous membrane system interconnected with the nuclear membrane (Schwarz & Blower, 2016) this pattern of expression is as expected and demonstrative of ER specific staining. In comparison the expression pattern of the CALR is very similar (Figure 3.2A-C) with a clearly defined ER with increased staining localised to one side in a similar manner to that observed in PDI stained HT1080 cells (Figure 3.2G). There does however appear to be some staining that may be cytoplasmic (indicated by arrows Figure 3.2A-C). The second purpose of the experiment was to determine the titration of the antibody at which consistent results could be obtained. Three dilutions were initially selected, 1:200 (Figure 3.2A), 1:500 (Figure 3.2B) and 1:1000 (Figure 3.2C). As can be seen in Figure 3.2(A-C) all antibody dilutions produced the expected staining pattern. At 1:200 dilution (Figure 3.2A) the staining appears very intense and there doesn't appear to be any non specific staining. A similar result was obtained with the 1:500 dilution (Figure 3.2B). The expression pattern was still clear although it appeared less intense. At an antibody dilution of 1:1000 (Figure 3.2C), the expected ER staining pattern was visible however the results were not consistent across the slide with some cells being more intensely stained than others. Taken together this suggest that a dilution of 1:500 provides a consistent result for use in further experiments. Finally, as cervix/vaginal cell lines were the primary cell type to be used in t he experiments it was also important to test if similar

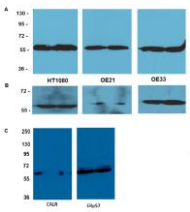

Figure 3.2 Detection of CALR in Oesophageal Cell lines. **(A)** Lysates from HT1080 and from OE21 and OE33 cells were prepared and ran on a 10% SDS-Page gel under reducing conditions before transfer to a PVDF membrane and incubation with a 1:1000 dilution of the CALR antibody (n=2). **(B)** After blotting the membrane was re-probed with PDI as a loading control **(C)** A second experiment was conducted with OE19 cells, using the same method and conditions before blotting with CALR and ERp57 (n=1).

results could be obtained with the oesophageal cell lines to be used. OE19 (Figure 3.2D), OE21 (Figure 3.2E) and OE33 (Figure 3.2F) were also stained with a 1:500 dilution of the antibody against CALR and compared against PDI (PDI replicates not shown). All these oesophageal cell lines showed a similar expression pattern to that observed with the HTI160 cells and this was comparable to that of PDI in the same cell lines, demonstrating that the CALR antibody appeared to detect CALR consistently across multiple cell lines. However, it was noted that some of the staining may extend beyond the ER (Figure 3.1A-C and E), this is consistent with the suggestion that while CALR is predominantly ER localised there were some foci or punctae in some cells, and the relevance of these remains to be investigated

3.2.3 The CALR antibody gives a strong, well defined signal in Western blotting in oesophageal cell lines.

Experiments from the Okabe group have been performed using CALR on lysates taken from sperm collected from the epididymis and vas deferens of mice (Nauss, et al., 2011). It was therefore important to determine if the antibody would detect the presence of CALR when blotted against lysates taken from the human cell lines to be used. Initially only lysates were generated from HTI160, OE21 and OE33 cell lines by the standard method (see Chapter 2, 2.5) and equal amounts of protein per well were run on a 10% SDS-page gel, under reducing conditions before transfer to PVDF membrane. Membranes were blocked then probed with a 1:1000 dilution of the CALR antibody for 1 hour at room Figure 3.3A), developed to see if there was any CALR signal and then re-probed with a 1:1000 dilution of an antibody against PDI(Figure 3.3B) as a loading control. From the experiment it could be seen that the antibody strongly and specifically detected the presence of CALR in all the cell lines tested (Figure 3.3A). There appeared to be slightly less expression of CALR in OE21

cells but a re-probe of the membranes with the PDI antibody (Figure 3.3B) showed that protein loading may not have been equal across all the lanes. After the initial run of experiments it was decided to include OE19 cells in the analysis. Lysates generated from OE19 cells were, using the same method as used to generate lysates from HTL060, OE21 and OE33 cells and ran under the same condition as the previous experiment. The membrane was probed with a 1:1000 dilution of the CALR antibody (as used initially) alongside a commercial antibody against E-RpS7(cell signalling G117) (Figure 3.3C). CALR was detected in the OE19 cell line, although the signal was fainter than was previously expected from the other cell lines tested (Figure 3.3A). ErpS7 however gave a strong signal suggesting that the poor signal from CALR may have been due to an issue with transfer or detection.

3.2.4. The CALR antibody shows strong expression in the exocrine pancreas but not in the islets of Langerhans.

Human pancreatic tissue was incubated with a 1:200 dilution of the CALR antibody, DAB stained and then co-stained with haematoxylin (Figure 3.4). The overall staining was even across the tissue (Figure 3.4A) with CALR protein expression present in the glandular cells of the exocrine pancreas but not the islets of Langerhans. This result appears to be consistent across all the areas of the tissue viewed (Figure 3.4 (B-C). This result compares favourably with data obtained from the human protein atlas, which shows medium intensity of CALR staining in the exocrine pancreas and no staining in the islets of Langerhans in the majority of the tissue they tested (Uhlen, et al., 2017). In contrast, Omikorede *et al* showed an significant increase in islet CALR expression between lean and obese Zucker rats. They showed very low very low levels of CALR expression in lean mice which was significantly increased in obese mice in response to ER stress/UPR activation (Omikorede, et al., 2013).

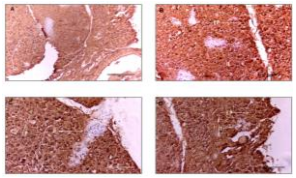

Figure 3.4 Detection of CALR in Human Pancreatic Sections, Scale bars represent 200µm. (EP) Exocrine Pancreas, (IL) Islets of Langerhans. Human pancreas tissue sections were stained with the antibody against CALR (n=2) and then counterstained with haematoxylin then imaged with at ×5 magnification **(A)** and ×20 magnification **(B-D)**

This experiment along with the previous Western blotting data and the immunofluorescence experiments suggest that the CALR polyclonal antibody is appropriate for Western blotting, immunofluorescence and in immunohistochemistry for the detection of human calreticulin in cell lines and tissues.

3.2.5. Validation of CANX expression using an antibody previously untested in human cell lines and tissues.

The anti calnexin antibody, also raised in rabbit and provided as a kind gift by the Okubo group was also tested. Initial Immunofluorescence experiments were conducted with HTr1040 cells using three antibody dilutions (1:200, 1:500 and 1:1000) gave variable results (Figure 3.5), but did confirm that a 1:500 dilution of the CANX antibody (Figure 3.5B) was worth investigating further (Figure 3.5D). Going forward, it was decided to use a 1:500 dilution of the CANX antibody to test its expression in the oesophageal cell lines OE21(Figure 3.6E) and OE33 (Figure 3.6F). Expression of CANX in OE21 and OE33 cells was comparable, in most cases with that of PDI (Figure 3.6G) and was suggestive of ER staining. There appeared to be none of the possible cytoplasmic staining observed with the CALR antibody, which was as expected given that CANX is ER membrane bound (Helenius, et al., 1997). The titration of the CANX antibody was finally re-visited using OE19 cells (Figure 3.6 A-C) although the staining pattern was more difficult to see, in OE19 cells due to their propensity to clump together.

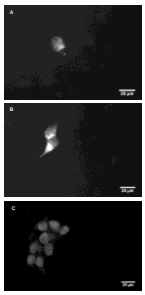

Figure 3.9. NTI-985 cells stained with anti- CA50 antibody and Hoechst at x40 magnification (n=1), at dilutions of 1:200 (n=1) **[A]**, 1:500 (n=1) **[B]** and 1:1000 (n=1) **[C]**. **Scale bars represent 25µm**

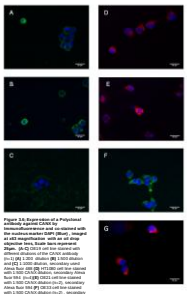

Figure 3.6. Expression of a Polyclonal Antibody against CA125 in Ovarian Cancer Cell Lines. **Cells were fixed with formaldehyde and co-stained with the nucleus-marker DAPI (Blue). Images were captured using a 40x objective lens. Scale bars represent 20µm.** **(A-C)** OSC19 cell line stained with **(A)** 1:100 dilution, secondary used (n=1) **(B)** 1:300 dilution **(C)** 1:600 dilution and **(D)** 1:1000 dilution, secondary used (n=1). **(D-F)** OSC19 cell line co-stained with 1:500 CA125 titration, secondary Alexa fluor 594. (n=2)**(G)** OSC3 cell line stained with 1:500 CA125 dilution (n=2) , secondary Alexa fluor 594 **(H)** OVCA Lod line stained with 1:500 CA125 dilution (n=2) , secondary Alexa fluor 594 **(I)** HGSE cell line stained with 1:500 (n=1) PDI dilution , secondary Alexa fluor 594

The experiment did confirm that, in OE19 cells, CANX appeared to be specifically associated with the ER and nuclear membrane and that a 1:500 dilution provided the best results, , although co-staining experiments would be required to determine the extend of co-localisation with other ER resident proteins.

3.3.6 The CANX antibody detects CANX by Western blotting in human oesophageal cell lines.

Like the CALR antibody it was important to determine the behaviour of the CANX antibody in Western blotting of lysates of the same cell lines that were tested with the CALR antibody. Therefore, SDS-PAGE was carried out using the same lysates generated from the HTs080, OE21 and OE33 cell lines that were used to examine the CALR antibody. Lysates were run on a 10% gel and proteins were transferred to PVDF membrane and blotted with a 1:1000 dilution of the CANX antibody (Figure 3.7A) developed and then re-probed with a PDI antibody as a loading control (Figure 3.7B). Additionally the CANX antibody was also tested using the OE19 cell line at the same time as the CALR antibody was tested (Figure 3.7C). From the first experiment (Figure 3.7A and B) it can be seen that the CANX antibody produced a well-defined signal in all three cell lines: interestingly there appears to be a second band, expressed in the OE33 cell lines but apparently absent in the HTs080 and OE21 cell lines. This second band was also seen faintly in the OE19 cell line when this was tested (Figure 3.7C). At first it was thought that this may be an experimental error caused by a slipping of the film during exposure to the ECL. However when taking into consideration the expression of ERp57 and the single band expressed by CALR (Figure 3.3C), which were loaded on the same SDS-page gel, then it is possible that the observed band is a low abundance truncated form of

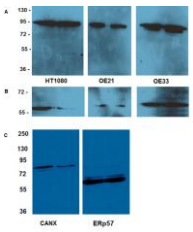

Figure 3.7 Detection of CANX in Oesophageal Cell lines, (A) Lysate, from HT1080 and from OE21 and OE33 cells were prepared and ran on a 10% SDS-Page gel under reducing conditions before transfer to a PVDF membrane and incubation with anti-CANX primary antibody (PC). **(B)** After blotting the membrane was re-probed with PVC ran a blot by re-probing the CANX blots (data not with OE19 cells (n=2), using the same method and conditions before blotting with CANX and ERp57.

CANX expressed in the OE33 and in OE19 cell lines which is not present in the OE21 cell line. The OE21 cell line was derived from an upper oesophageal squamous cell carcinoma, where as both the OE19 and OE33 cell lines were originally derived from adenocarcinoma cells taken from the lower oesophagus (see Chapter 2, 2.2) which may suggest that some form of post translational modification occurs to CANX in the OE19 and OE33 cells that doesn't happen in the OE21 cells.

3.2.7. CANX shows strong expression in the human exocrine pancreas

In the same manner as the tissue sections were stained for CALR (Figure 3.4), human pancreatic tissue was incubated with a 1:200 dilution of the CANX antibody, DAB stained and then co-stained with haematoxylin (Figure 3.8). Overall the staining was even across the tissue, indicating high expression of CANX particularly in the exocrine pancreas (Figure 3.8A). There was weaker expression in the blood vessels (Figure 3.8D), as indicated by lighter staining, and only some of the pancreatic ducts appeared to be expressing CANX (Figures 3.8B compared to Figure 3.8D).The islets of Langerhans appeared not to be expressing CANX (Figure 3.8DC which is in conflict with the data generated by the human protein atlas which suggests that, with the HPA009410 (Sigma), HPD09696 (Sigma) and sc-46669 (Santa Cruz Biotech), antibodies used CANX expression in the islets appeared to be medium to high (Uhlen, et al., 2017). Comparative staining with different CANX antibodies would be required to resolve this issue, but was not within the scope of this thesis.

In summary the both the CALR and CANX antibodies performed well across a range of methods and with various cell lines and tissues, validating the methodology

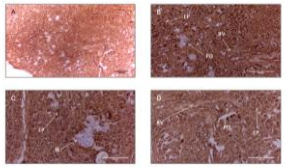

Figure 3.9 Detection of CAM in Human Pancreatic Sections. Scale bars represent 200µm. (DP) Exocrine Pancreas, (IL) Islets of Langerhans, (BV) Blood vessels, (PD) Pancreatic Ducts. Human pancreas tissue sections were stained with the antibody against CAM (Ha-4) , counterstained with haematoxylin and then imaged with at ×4 magnification (A) and ×20 magnification (B–D).

Investigation of the Expression Profile of GPx7

4.1 Introduction

As was briefly discussed in Chapter 1, there is a possible link between dysfunction of ER resident chaperones and the transition of the normal squamous epithelium of the oesophagus to BO and ultimately, in some cases, to OAC.

4.1.1 The Glutathione Peroxidase family in Barrett's Oesophagus.

Members of the GPx family of proteins have been shown to have a role in oxidative protein folding, disulphide bond formation and the response to stress in the ER (Chapter 1.15). The glutathione peroxidase, GPx8 has been shown to have a role in preventing the leakage of ERO1α generated H_2O_2 from the ER into the cytosol in HEK293 cells (Rumming, et al., 2014). In permafgrost BO loss of GPx3 by hypermethylation of its promoter region (Lee, et al., 2005) gave rise to an accumulation of intracellular ROS which may favour the development of OAC. Additionally, there is evidence that GPx7 may be silenced by location specific methylation in OAC (Peng, et al., 2014). Furthermore GPx7 has been implicated in the control of downstream elements of the NF-κβ inflammatory pathway, such that down regulation of GPx7 may result in the activation of NF-κβ signalling via TNF-α (Peng, et al., 2014). There is strong evidence that TNF-α and other NF-κβ mediated proinflammatory cytokines, such as IL-8 and IL-1β are elevated in BO and OAC (Tselepis, et al., 2002) (O'Riordan, et al., 2005).

Finally over-expression of GPx7 provided protection against bile acid or H_2O_2 induced oxidative stress in the oesophageal cell lines BAR-T and CP-A and reduced oxidative DNA damage and double strand breaks (Peng, et al., 2011). Further, expression of GPx7 may have a role as a tumour suppressor. Peng et al showed that the knockdown of GPx7 expression of in HET1A, an immortalised normal

oesophageal cell line resulted in an increase in growth, a decrease in the tumour suppressors p73, p27, p21 and p16 and an increased deactivation of retinoblastoma protein (Rb) by phosphorylation. Conversely the expression of GPx7 in OE33 cells resulted in reduced phosphorylated Rb and an increase in p73, p27, p21 and p16 (Feng, et al., 2014). This evidence suggests that, in BO disruption of the proteins of the GPx family may play a role in the pathogenesis of Barrett's Oesophagus and in the transition from stable BO to OAC.

4.2 Expression of GPx7 in immortalised cell lines

4.2.1 Immunofluorescence studies of GPx7

Peng *et al* claimed that GPx7 was down regulated in BO and OAC (Peng, et al., 2014). In order to study GPx7 a number of experiments were undertaken. Initially, a panel of immortalised cell lines were stained for GPx7, with PDI as a control, in order to determine if GPx7 was expressed and whether that expression was localised to the ER (Figure 4.1). All the cell lines used were immortalised cancer cell lines derived from different cancer types, HT1080 from a fibrosarcoma, HeLa from cervical cancer, OE21 from a squamous cell carcinoma of the upper oesophagus, OE33 cells from an adenocarcinoma of the lower oesophagus and finally OE19 cells, that were derived from an adenocarcinoma of the gastric cardia/oesophageal gastric junction (see Chapter 2, section 2.2).

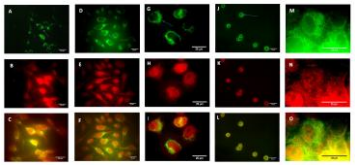

Figure 3.1: Cellular Expression of GPx7 by immunofluorescence, imaged at x63 magnification with an oil-drop objective lens. All antibody dilutions at 1:200, scale bar represents 10µm. Human embryonic kidney cells (HEK293) transfected with GPx7 plasmid (**C**) (n=2). **(C-E)** HEK293 cells stained with anti-GPx7 contained with anti-PDI (**C**) (n=2). **(E-G)** HEK293 cells stained with anti- PDI (**E**), anti-GPx7 (**F**) anti-GPx7 contained with anti-PDI (**G**) (n=3). **(H-J)** CB33 cells stained with anti-PDI (**H**), anti-GPx7 (**I**) anti-GPx7 contained with anti-PDI (**J**) (n=1). **(K-M)** CB33 cells stained with anti-PDI (**K**), anti-GPx7 (**L**) anti-GPx7 contained with anti-PDI (**M**) (n=1). **Arrow indicate ER location**

Each cell line was cultured to 70-80% confluence then stained with a polyclonal antibody against PDI with Alexia fluor 488 (green) and a commercial monoclonal GPx7 antibody with Alexia fluor 594 (red). Figure 4.1 shows the results for each cell line showing the 488nm wavelength channel, the 594 wavelength channel and a composite image. All the cell lines were positive for PDI expression (Figure 4.1A, D, G, J, M) and that expression appeared localised to the ER, with the exception of the HeLa cell line (Figure 4.1D) where the expression appeared predominantly localised to the ER but which also demonstrated a small degree of cytoplasmic staining. In contrast the expression of GPx7 appeared to be nuclear in all the cell lines, which is most apparent in the appropriate composite images for each cell line (Figure 4.1C, F, I L, O). From this series of experiments it appeared that Gpx7 was expressed in all cell lines, although in it did not appear to be localised specifically to the ER. This result raises the possibility that the GPx7 antibody could be detecting a non-specific protein or other members of the GPx family.

4.2.2 Gpx7 could not be detected in cell lines by Western Blotting.

In order to determine if the antibody was binding specifically to GPx7 cell lysates from each cell line were analysed by10% SDS-PAGE and then blotted for GPx7. Initially only HT1080, Hela, OE21 and OE33 cells were assessed (Figure 4.2A). According to the manufacturers product data sheet, for the mouse monoclonal antibody [2704] ab23727 (Abcam, 2017) an ~20kDa band was expected. Despite several attempts there was no detectable band in the HT1080, HeLa and OE21 lysates. However, in the OE33 lysate several bands were visible at ~55kDa and ~34kDa molecular weights. (Figure 4.2A).

m

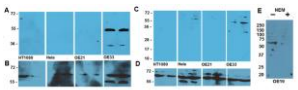

Figure 2.2. Western Blots of Oesophageal Cell Lines with a 1:1000 GPx7 antibody dilution. 10% SDS-PAGE blotted with Anti- GPx7(NT3350) n=2, Hela n=2, OE33 n=3, OE33 n=2 **(A)** and re-probed with 1:1000 anti-PDI (n=2) **(B)**. 12% SDS-PAGE blotted with anti-GPx7(NT3350) n=2, Hela n=2, OE33 n=2, OE21 n=2, OE19 n=2 **(C)** and re-probed with 1:1000 anti-PDI (n=2) **(D)**. 12% SDS-PAGE of OE33 cell lysates blotted with anti-GPx7 >> HEM (n=1).

Re-probing negative GPx7 negative membranes with anti-PDI indicated that overall the transfer was successful (Figure 4.2B). In order to control for possible fast migration of the GPx7 protein, the experiment was repeated using a 12% gel (Figure 4.2C). Again there were no visible bands at the 15kDa molecular weight marker, however the same 35 and 55 kDa bands appeared in the OE33 lysate as seen in the 10% gel experiment (compare Figure 4.2A, panel 4, with Figure 4.2C, panel 4).

Finally an experiment was conducted using OE19 lysates (Figure 4.2C) that had been lysed with and without 20mM NEM. This experiment was performed using a GPx7 polyclonal antibody gifted by the Wang Group (see Chapter 2, 2.1) (Wang, et al., 2014). Without NEM there was a clear strong band between the 55kDa and 75kDa molecular markers and faint signals at higher molecular weights. In the presence of NEM there was a decrease in the signal compared to the sample without NEM, in addition to the faint bands seen at higher molecular weights. In both plus and minus NEM samples there appeared a very slight spots at ~20kDa but it is not apparent if this is a true signal or not.

From the Western blotting data it appeared that GPx7 was not detectable in the cell lines tested, despite the abcam antibody giving a strong nuclear staining pattern by immunofluorescence. This appears to correlate with the published literature from Peng et al, which showed that, in OE33 cells, GPx7 expression was suppressed by site specific, promoter methylation at the transcriptional level. (Peng, et al., 2014). The appearance of bands at other molecular weights and the data taken from Immunofluorescence (see section 4.2.1 and Figure 4.1) strongly suggests that, in the absence of GPx7 non-specific binding is occurring. . Interestingly, recent data from the *human protein atlas* suggests that GPx7 may have a nucleolar localisation, from experiments using an independent antibody (ab HPA025829) (Uhlen, et al., 2017)

87

In order to ascertain if the observed signal seen, in Hela and CE23 cells (and later in the OE19 cell line) was non-specific binding, it was decided to transfect Hela cells with a GPx7 encoding cDNA, with the goal of analysing GPx7 expressing cells for their response to ER and bile acid stress. Hela cells were transfected (for protocol, see Chapter 2, 2.4) with a commercial Myc tagged GPx7 cDNA and along with an ERO-1α cDNA mutant (which had previously been successfully transfected into Hela cells) as a positive control. The cells were cultured to 80% confluence, in 6cm dishes containing 13mm glass coverslips before transfection with, lipofectamine 3000, using 2μg of the appropriate cDNA overnight. The coverslips were then removed, fixed and analysed by immunofluorescence (Figure 4.3). Non-transfected Hela cells were also imaged for comparison (Figure 4.3D). In the non-transfected cells the distribution of staining appeared non-specific, with background distributed throughout the cytoplasm. The staining in the transfected cells showed a tighter distribution, however it didn't appear strongly localised to the ER (Figure 4.3A). Staining of the myc tag (Figure 4.3B) showed that the cells had been transfected successfully as the presence of the myc was co-localised with that of the observed GPx7 staining (Figure 4.3C). By comparison the Hela cells transfected with ERO-1α show staining which appears more ER based (Figure 4.3E) when compared to the staining observed in the non-transfected Hela cells (Figure 4.3H). This is supported by the myc tag staining (Figure 4.3G) where there appeared to be myc staining in areas where there was no ERO-1α expression.

Overall it was difficult to detect GPx7 intransfected Hela cells.

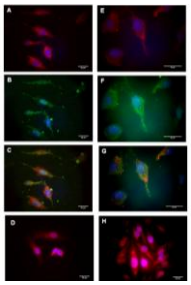

Figure 4.3 HeLa Cells stained with anti GPx7 antibody and HRI and ERO-1α antibody at x63 magnification using an oil drop objective lens, scale bar represents 20μm [ALL] **(A-C)** HeLa cells transfected with myc tagged GPx7 cDNA **(A)** transfected cells stained for GPx7 (red) and DAPI (blue) **(B)** transfected cells stained for myc (green) and DAPI (blue) **(C)** transfected cells stained for GPx7, myc and DAPI overlay **(D)** Non-transfected cells stained for GPx7. **(E-F)** HeLa cells transfected with myc tagged ERO-1α cDNA **(E)** transfected cells stained for ERO-1α (red) and DAPI (blue) **(F)** transfected cells stained for myc (green) and DAPI (blue) **(G)** Composite image showing ERO-1α, myc and DAPI overlay **(H)** Non-transfected cells stained for ERO-1α

4.2.3 GPx7 is expressed in leydig cells but was not detectable in human pancreas, Barrett's oesophagus or oesophageal, gastric tumour.

In an attempt to see if GPx7 was increased in BO and in oesophageal cancer human tissue was stained to detect GPx7. It has been suggested that GPx7 expression, may be high in the reproductive system (Uhlen, et al., 2017) (Ryser, et al., 2011) and so tissue obtained from rat testis was sectioned and stained for GPx7. In addition human pancreatic tissue was stained as a negative control alongside the human oesophageal tissue and the rat testis as the human protein atlas showed that pancreatic expression was low to none (Figure 4.4) (Uhlen, et al., 2017).

Pancreatic tissue was stained with DAB and haematoxylin only as a negative control (Figure 4.4A), for insulin as a positive control (Figure 4.4B) and for GPx7, using the anti-GPx7 antibody obtained from the Yang group (chapter 2.2.1) (Figure 4.4C). As expected from the literature (Uhlen, et al., 2017) GPx7 staining was practically non-existent throughout the pancreatic tissue with a few areas of weak brown staining which were likely to be DAB overdevelopment. The rat testis (Figure 4.4D) showed GPx7 expression in both the leydig cells and in the seminiferus ducts which also agrees with the literature (Ryser, et al., 2011). In the tissue sample of BO there appeared to be no expression of GPx7 in the stratified squamous epithelium (Figure 4.4E) although there was an indication of slight expression in the lamina propria. Other than expression in lymphocytes, which have a high expression of GPx7 (Uhlen, et al., 2017), there was a slight indication of GPx7 expression in the tumour tissue taken from the oesophageal gastric junction. However GPx7 did not appear to be localised to the tumour cells and may have been in the lamina propria although this wasn't clear given the disorder of the tissue. This appears to correlate with the

cellular data where GPx7 expression was not detectable in oesophageal cell lines, when analysed by Western blotting.

Taken together there did not appear to be any expression of GPx7 in lysates obtained from immortalised cancer cell lines. Similarly there did not appear to be any expression of GPx7 in tissue taken from patient samples of BO. However, there was an indication of expression of GPx7 in the stained rat testis which suggests that the antibody obtained from the Yang group could be suitable for visualising GPx7 expression in tissue under the right conditions. (Wang, et al., 2014).

m

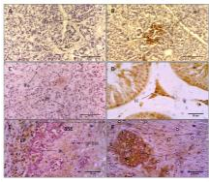

Figure 4.4 Expression of GPx7 in rat testis, human pancreas, BO and in an oesophageal-gastric junction tumour. **(A)** blood vessel, **(BP)** exocrine pancreas, **(PD)** pancreatic duct, **(L)** islets of langerhans, **(LC)** leydig cells **(LP)** lamina propria, **(SER)** stratified squamous epithelium **(BC)** basal cells, **(SC)** sertoli cells, **(SG)** seminiferous tubules, **(SM)** smooth muscle, **(V)** vacuole. colocal: x10 magnification **(B)** Human pancreas stained for duodenal-ating anti-NB antibody x10 magnification (n=2) **(C)** Human pancreas stained for GPx7 x10 magnification (n=2) **(D)** Rat testis stained for GPx7 x10 magnification (n=3) **(E)** Human BO tissue stained for GPx7 x40 magnification (n=3) **(F)** Human oesophageal-gastric junction tum our stained for GPx7 x40 magnification (n=3). Presence of lymphocytes suggested by morphology (Urban, et al., 2017)

Investigating the Expression of Prdx4 in the Oesophagus

5.1 Introduction

Prdx4 is an ER resident scavenger of H_2O_2 (Sevier & Kaiser, 2008) which, as discussed in Chapter 1, can utilise H_2O_2 to aid in disulphide bond formation (Tavender, et al., 2008). Prdx4 exists, in the ER, in a decameric form comprising of five Prdx4 dimers (Figure 5.1). Each Prdx4 polypeptide contains a single peroxidatic cysteine which can react with peroxide to become sulphenylated. The sulphenylated cysteine can then react with the resolving cysteine on the adjacent Prdx4 polypeptide in Prdx4 dimer to form a disulphide bond, which is then available to be donated to a reduced PDI family member (Sullivan & Ellgaard, 2011). It has been suggested that, under normal conditions, members of the GPx family are responsible for the prevention of H_2O_2 accumulation from oxidative protein folding within the ER and that Prdx4 assisted detoxification only becomes applicable when levels of H_2O_2 in the ER are maximised (Ramming, et al., 2014). As discussed in Chapter 4, in BO and OAC there is evidence to suggest that the H_2O_2 scavenging capacity of the GPx, such as GPx7, is impaired and so it then becomes important to examine how the activity and regulation of Prdx4 is affected.

5.2 Prdx4 expression in oesophageal cell lines

Initial experiments to validate antibodies and confirm the expression of Prdx4 were carried out in the HT1080 cell line using immunofluorescence. HT1080 cells were cultured to approximately 70% confluence on 13cm glass cover slips, fixed and stained with either Prdx4 or PDI, as a positive control (Figure 5.2). Comparing the cells stained with PDI (Figure 5.2A) with those stained for Prdx4 (Figure 5.2B), Prdx4 appeared to be expressed and localised to the ER. Next lysates from confluent HT1080 cells and mouse kidney, were run on a 10% SDS-PAGE gel for

analysis of Prdx4 expression by Western blotting (Figure 5.2C) with PDI expression as a positive control (Figure 5.2C, lanes 5 and 6). Initially, no signal could be detected Prdx4 but the lanes stained for PDI showed that transfer had been successful. Staining of the membrane with ponceau S (Figure 5.2D), confirmed that the transfer had been successful, although some degradation had occurred in the mouse kidney lysate probably due to the freezing or thawing process.

m

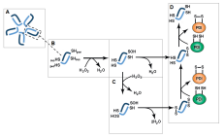

Figure 5.1 The Reaction Cycle of Prdx1. Prdx1 exists as a decamer consisting of 5 dimers **(A)** Each polypeptide in a Prdx1 dimer contains a peroxidatic (per) and a resolving (res) cysteine **(B)** The peroxidatic cysteine reacts with hydrogen peroxide and becomes sulphenylated. This sulphenylated cysteine can react with the resolving cysteine on the opposite polypeptide, forming a disulphide bond and releasing water. In reduced PDI family member **(D)** As each Prdx1 polypeptide contains a peroxidatic and resolving cysteine it is possible that a sulphenylated cysteine can react further with hydrogen peroxide forming a sulphenylated cysteine on each polypeptide, which can further go on to form two disulphide bonds **(C)**. adapted from (Butterfield & Hägglund, 2011)

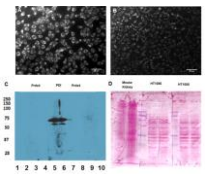

Figure 1.2 Pvrl-2 expression in HT1080 cells.[A] Immunofluorescence of HT1080 cells stained for PVL scale bar represents 25 µm (n=2). **[B]** Immunofluorescence of HT1080 cells stained for Probe-6, scale bar represents 25 µm (n=2). **[C]** SDS-page under reducing conditions ran on a 10% gel, lanes 2and 3 contain mouse kidney lysate, lanes 5,8,9 and 10 HT1080 lysate (n=3). **[D]** PVL2 exercise stained with Probe-6 (n=3).

In order to determine if Prdx4 was expressed in oesophageal cell lines, immunofluorescence was performed on OE19 and OE33 cells (Figure 5.2). OE19 cells were stained with PDI (Figure 5.3A) and Prdx4 (Figure 5.3B). Comparing the OE19 cells stained with Prdx4 with those stained with PDI, as a positive marker of ER staining, Prdx4 appeared to be localised specifically to the ER. Comparing Prdx4 expression in OE33 cells (Figure 5.3D) with OE33 cells stained for PDI (Figure 5.3C) again the expression of Prdx4 appeared to be localised specifically to the ER. This was similar to the result obtained in HTU580 cells (Figure 5.2). An OE19 cell lysate was run on a 12% polyacrylamide gel under reducing conditions, with and without the presence of NEM to trap disulphide bonds. Prdx4 was detected at the expected 25 kDa band (Figure 5.3E) and in addition to this a faint band was detected around the 50 kDa marker in the OE19 lysate with NEM. In order to determine if this was a repeatable result, OE19 and OE33 cell lysates were run with and without NEM under reducing conditions (Figure 5.3F) and non-reducing conditions (Figure 5.3G). It was found that Prdx4 was detected at the expected molecular mass of ~25 kDa in the OE19 and OE33 cell lysate, under reducing conditions. In addition in OE19 cells a clearly defined band at ~50kDa and a third band was detected at around 75 kDa (Figure 5.3F). In contrast, the 50 kDa and 25 kDa bands were absent from OE33 lysates.

When reduced, by its interaction with H_2O_2, Prdx4 can bind to PDI to aid disulphide bond formation within PDI (Tavender, et al., 2008). It is therefore possible that, in the reduced samples, the NEM has trapped the interaction between PDI and Prdx4 (Figure 5.2F).

≡

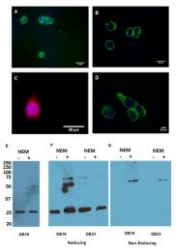

Figure 5.3 Expression of Prdx4 in OE19 and OE33 cells (A) Immunofluorescence of OE19 cells stained with PDI (green) and DAPI (blue), scale bar represents 25 µm (n=2). Immunofluorescence of OE19 cells stained with Prdx4 (green) and DAPI (blue), scale bar dependent on 25 µm (n=2). **(C)** Immunofluorescence of OE33 cells stained with PDI (red) and DAPI (blue), scale bar represents 25 µm(n=2). **(D)** Immunofluorescence of OE33 cells stained with Prdx4 (green) and DAPI (blue), scale bar represents 25 µm(n=2). **(E)** SDS-page of OE19 cell lysate +/- NEM under reducing conditions (n=2). **(F)** 5-15 page of OE19 and OE33 cell lysates +/- NEM under reducing conditions(n=2). **(G)** SDS-page of OE19 and OE33 lysates +/- NEM under non-reducing conditions (n=2).

Similarly as native PrdxI exists as a toroid shaped decamer (Tavender, et al., 2008) (Wang, et al., 2012), within the ER, the observed bands seen in the non-reducing gel, in the presence of NEM, could possibly be trapped in a reaction intermediate (possibly a dimer).

5.3 Expression of PrdxI in human tissue

With the observed expression of PrdxI in the oesophageal cell line models of BO and OAC it was important to see if expression could be detected in human tissue samples of BO and OAC, compared to samples taken from normal oesophageal and gastric tissues. Samples of normal oesophagus, normal gastric, BO tissue and tissue taken from an oesophageal gastric junction tumour were therefore immunohistochemically stained for PrdxI. In addition, as pancreatic expression of PrdxI is high (Uhlen, et al., 2017), human pancreatic tissue was also stained as a positive control (Figure 5.4). As expected, in the pancreatic, expression of PrdxI was high in the exocrine pancreas and low to none in the islets of langerhans tissue (Figure 5.4A). PrdxI was expressed in the normal oesophageal tissue (Figure 5.4C) compared to control (Figure 5.4 B) however expression appeared low when comparing it to the PrdxI expression in normal gastric tissue (Figure 5.4D). In the patient samples of BO there was a disparity in the level of staining between those areas which had the appearance of squamous epithelium and those which contained cells with the morphology of gastric columnar cells (Figure 5.4E and F). This appeared consistent between different samples, allowing for between patient variation.

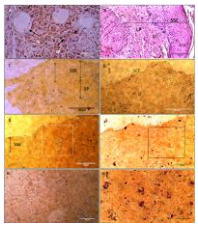

Figure 5.2 Human Tissue expression of Pnlip1. **(A)** Human Pancreas stained for Pnlip (n=3). **(B)** Normal oesophagus control. **(C)** Normal oesophageal tissue stained for Pnlip1 (n=3). **(D)** Normal gastric tissue stained for Pnlip1 (n=3). **(E and F)** BO tissue from two separate patient samples, boxed area indicates presence of gastric -like glandular tissue (n=3). **(G and H)** Oesophageal-gastric junction- tumour from two separate patient samples , (n=2). **Key: (SL)** Islets of Langerhans **(SP)** Exocrine pancreas **(SSE)** Stratified squamous epithelium **(LP)** Lamina propria **(BC)** Basal cell **(DSC)** Differentiating squamous cell **(SCE)** Stratified columnar epithelium **(G)** Gland.

In the tissue samples taken from patients with an oesophageal-gastric-junction-tumour (Figure 5.4 G and H) the pattern of staining appeared inconsistent, there was evidence that some areas may have a darker staining, which may indicate localised areas of increased Prdx4 expression, however this wasn't clear in one of the patient samples (Figure 5.4G). In another sample, however, there were clearly observable areas of staining, possibly indicating areas with high expression of Prdx4 (Figure 5.4H). This correlates with the observations that Prdx4 expression in breast and prostate cancers is increased in areas of carcinoma compared to non-tumour tissue (Hess, et al., 2006). Similar increases in Prdx4 expression have also been found in Oral Cavity Squamous Cell Carcinoma and in Glioblastoma multiformes, an aggressive brain malignancy (Chang, et al., 2011) (Kim, et al., 2012).

Taken together, the data suggest that Prdx4 expression is worth pursuing as a possible marker of GI cancer in a larger scale study.

Investigating AGR2 a Novel PDI family Member

6.1 Introduction

Anterior Gradient 2 (AGR2) is a member of the PDI family. Over-expression of AGR2 has been linked to various roles in a number of cancers, as discussed in Chapter 1 (Chapter 1.16), reviewed in (Brychtova, et al., 2011). Research into AGR2 has suggested that it may also have a role in BO and its transformation into OAC through the silencing of the tumour suppressor p53 (Fichter, et al., 2004).

AGR2 is involved in the production of intestinal mucus (Park, et al., 2009) and has been linked to the response to stress in the ER (Zhang, et al., 2007) (Zhao, et al., 2010). Research has shown that AGR2 can interact with BiP/GRP78 and that this interaction is dependent on AGR2 dimerisation (Ryu, et al., 2013). However, the exact role that AGR2 has in the ER stress response is unclear. There is also evidence to suggest that it may also form complexes with other ER resident proteins either as a monomer or as an interaction between a target protein and its homodimer (Clarke, et al., 2014).

6.2 AGR2 Expression in Human Tissue Sections

Tissue blocks of normal oesophageal, normal gastric, BO and OAC from human patients, were sectioned, mounted on polarised microscope slides and then stained for AGR2 (Figure 6.1). AGR2 was present in normal gastric tissue, in the columnar glandular cells (Figure 6.1B) but was not present in normal oesophageal tissue (Figure 6.1A). The tissue sections taken from the oesophagus of patients presenting with BO (Figures 6.1C and 6.1D) show a mixed morphology with the presence of gastric columnar cells (Figure 6.1C) and glandular tissue (Figure 6.1D). AGR2 expression appeared high in the columnar glandular cells (Figure 6.1C) and in the glandular tissue (6.1D) while remaining low, in comparison, in the normal squamous

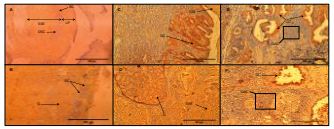

Figure 5.1 Histological Staining of Human Tissue Sections with 1.25X and 10X Lenticular or 4X magnification. Scale bars represent 200µm. **(A)** Normal Human Oesophagus stained for CK8/18 (n=1). **(B)** Normal Gastric tissue stained for CK8/18 (n=1). **(C)** Barrett's Oesophagus tissue stained for AGR2 (n=2). **(D)** Barrett's Oesophagus tissue stained for AGR2 (n=1). **(E)** Oesophageal-Gastric Junction Tumour tissue stained for AGR2 (n=1). **(F)** Oesophageal-Gastric Junction Tumour tissue stained for AGR2 (n=1). **(G&I)** Modified squamous epithelium **(LP)** Lamina propria **(BC)** Basal Cell **(DSC)** Differentiating squamous cells. **(SC)** Glandular cells (Simple columnar epithelium). **(G)** Glands. **(GAC)** Oesophageal adenocarcinoma. RO tissue and OG27 each taken from two different patient samples.

epithelium (Figures 6.1C and 6.1D). In the tissue sections taken from patients presenting with OAC (Figures 6.1E and 6.1F), AGR2 expression appears confined to the glandular cells overall however there is some suggestion of AGR2 expression in the undifferentiated cellular region of one of the samples (Figure 6.1F).

From the experiment it appears that AGR2 is expressed in the columnar epithelium of gastric tissue but not normally expressed in the oesophagus, consistent with the literature. In comparison AGR2, in BO, is only expressed where the squamous epithelium has transitioned into glands or columnar epithelium. This is probably due to AGR2's involvement in the production of mucus. In the samples of OAC, AGR2 is expressed mostly in the columnar cells but there is some suggestion that AGR2 may also be expressed in the tumour mass.

6.3 Expression of AGR2 in Oesophageal cell lines

In order to determine if AGR2 was also expressed in oesophageal cell lines. OE19 and OE33 cells were cultured to approximately 70% confluence, on 13mm glass cover slips. The cells were then fixed with 4% paraformaldehyde and then permeabilised in ice-cold methanol before blocking for an hour and then incubated overnight at 4°C with either an anti-AGR2 antibody or PDI antibody as a positive control of ER localisation. Each coverslip was then incubated with an appropriate fluorescent secondary antibody and co-stained with DAPI (Figure 6.2). Comparing OE19 cells stained with AGR2 (Figure 6.2B) to OE19 cells stained with anti-PDI (Figure 6.2A) showed that, in OE19 cells, AGR2 is localised to the ER. In comparison the expression of AGR2 in OE33 cells was only present in a few cells (Figure 6.2D) and those cells which showed some expression did not present with

the characteristic ER staining shown in the OE19 cells stained with the anti PDI antibody (Figure 6.2C).

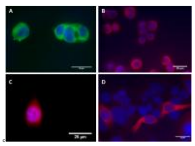

Figure 6.2 Expression of AQP2 in oesophageal cell lines. OE19 and OE33 cells stained with either anti AQP2 or anti PDI antibody. **(A)** OE19 cells stained for PDI (Ex1) **(B)** OE19 cells stained for AQP2 (Ex1) **(C)** OE19 cells stained for PDI (Ex2) **(D)** OE33 cells stained for AQP2(Ex 2). Nuclear co-staining with DAPI. **Scale bars represent 20µm**

Comparing the expression of AGR2 between the OE19 and OE33 cell lines showed that the expression of AGR2 was strongly expressed in the OE19 cell line (Figure 6.2A) compared to OE33 cells (Figure 6.2D). In the OE19 cell line AGR2 was expressed in each cell where as in the OE33 cell line only a very small amount of cells appeared to be expressing observable amounts of AGR2.

To investigate this further cell lysates of OE19 and OE33 cells were separated by SDS-PAGE under reducing conditions and Western blotted with an anti-AGR2 antibody (Figure 6.3A). The OE19 cell lysate showed a good signal at the expected molecular weight which was absent in the OE33 lysate. Based on this result, the SDS-PAGE was repeated, using OE19 cell lysate, under both reducing and non-reducing conditions. To explore whether AGR2 formed any complexes with other protein OE19 cell lysates were run with or without NEM to preserve disulphide bonds (Figure 6.3B). Under reducing conditions, without NEM, the result of the experiment was similar that seen in Figure 6.3B lanes 1 and 2. Under non-reducing conditions, without NEM, only the expected bands appeared (Figure 6.3B lanes 5 and 6). However in the samples with NEM bands are visible at 37 kDa, ~50 kDa and around the 75 kDa molecular marker (Figure 6.3B lanes 7 and 8). In the samples run under non-reducing conditions, with NEM, the band seen at 37 kDa could possibly be AGR2 in a dimeric form, as seen by Ryu et al and if so then it is possible that another of the bands may be an association with BiP (Ryu, et al., 2012).

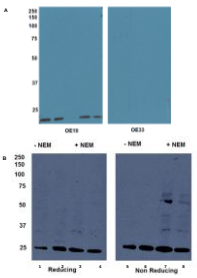

Figure 6.3 SDS-PAGE and Western blotting of AQR2 in oesophageal cell lines. A. OE19 and OE33 lysates run on a 12% gel under reducing conditions (n=2). **B.** OE19 lysates run under reducing conditions without NEM (lanes 1 and 2) and with NEM (lanes 3 and 4) and run under non-reducing conditions, without NEM (lanes 5 and 6) and with NEM (lanes 7 and 8) (n=2).

However the presence of more bands than those previously seen suggests that AGR2 can form multiple complexes with other ER resident proteins.

In order to determine if the observed AGR2 interactions were redox dependent OE19 cells were cultured to confluence and then treated with redox modifying reagents. To establish reducing conditions, OE19 cells were cultured in three 6cm dishes, one dish was used as a control, one was treated with 5mM DTT and one dish was first treated with 5mM DTT for 5 minutes then washed and incubated in media for a further 10 minutes. This was done to see if removal of the reducing conditions resulted in a return to the control state, which would indicate that the complex formation was reduction dependant. Similarly the experiment was repeated under oxidising conditions with 5mM Diamide to determine if the complex formation was oxidation dependant. After each treatment, including the control, samples were washed with 20mM NEM for 5 minutes, to preserve any disulphide bonds then lysed and analysed by SDS-PAGE under non-reducing conditions with NEM (Figure 6.4).

In the Western blot of the samples under reducing conditions (Figure 6.4A), the control samples exhibited a similar pattern of bands as previously seen (Figure 6.3B). These bands disappeared when the OE19 cells were treated with 5mM DTT leaving only the main AGR2 monomer band. When OE19 cells were treated with 5mM DTT and then allowed to recover by incubation for a further 10 minutes with untreated media there was a noticeable return of some of the extra bands. The disappearance and then recovery strongly suggests that the interactions disulphide are redox dependant.

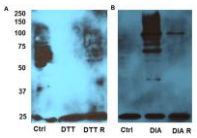

Figure 5.3 SDS-PAGE and Western blot analysis of ADM2 in cells treated with redox modulators. Cells were lysed and separated by SDS-PAGE under non-reducing conditions. **A** HEK293 cells were either washed then incubated with 5mM DTT or incubated with 5mM DTT then washed and incubated for a further 10 minutes with untreated media (DTT R) (n=2). and **B** OE19 cells were either washed then incubated with media as a control (Ctrl), incubated with 5mM Diamide (DIA) or incubated with 5mM Diamide then washed and incubated for a further 30 minutes with untreated media (DIA R) (n=2).

The experiment was then repeated with Diamide as an oxidation agent (Figure 6.4B). Examination of the Western blot showed a similar control pattern of bands however they were fainter than seen in the previous experiment. The addition of 5mM Diamide to OE19 cells clearly showed an increase in the number and signal strength of the extra bands. Allowing the OE19 cells to recover for 10 minutes after Diamide treatment showed a return to the band pattern seen in the control, with the exception of a strong band at 100 (Figure 6.4B). This suggests that oxidation increases the formation of extra bands.

These experiments demonstrate that the observed extra bands are redox dependant and that these extra bands represent AGR2 complex formation. This suggests that the ability of AGR2 to form complexes with other proteins is redox dependant and suggests a role for AGR2 in oxidative protein folding despite the lack of a conventional CGHC motif in the a domain.

PDI is involved in oxidative protein folding pathways in the ER. It was therefore logical to see if it was one of the client proteins that complexed with AGR2. To investigate this an immunoprecipitation was prepared. Protein A sepharose beads were incubated with anti-PDI antibody before immunoprecipitating PDI from OE19 cell lysate. The bead-lysate mixture was centrifuged, washed and the beads collected in sample buffer, as detailed in Chapter 2.2.7. The immunoprecipitate was then analysed by SDS-PAGE, on a 12% polyacrylamide gel under reducing conditions, without NEM, alongside a mixture of lysate, anti-PDI antibody (MA3-019, Bioreagents) and beads and input OE19 lysate (Figure 6.5) prior to Western blotting with an anti-AGR2 antibody.

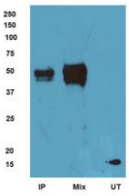

Figure 4.5 Immunoprecipitation of OE19 cell lysate s.
OE19 cell lysate incubated with Protein A sepharose beads and rat anti-PDI antibody in PBS lysate buffer (**IP**). A Mix of OE19 lysate, anti-PDI antibody and sepharose beads (**Mix**) and OE19 lysate only (**UT**) were run on a non-reducing conditions, without MEM, on a 12% acrylamide gel then western blotted for AGR2 (n=1).

AGR2 was detected in the untreated lane as expected but was not present in the mix or P lanes (Figure 6.5) suggesting that, based on this experiment, PDI and AGR2 do not form detectable complexes in the ER.

In summary AGR2 was found to be expressed in normal gastric tissue but not in the normal oesophagus. AGR2 expression in patient samples of BO was found to be confined areas that had undergone the transformed into gastric like tissue. In OAC, AGR2 expression was found both inside and closely associated with the tumour mass which could suggest that, in OAC, the tumour produces and secretes AGR2.

Examining AGR2 expression in oesophageal cell lines, AGR2 was detected in OE19 cells but not in OE33 cells, when analysed by Western blotting. In immunofluorescence, AGR2 was found to be expressed strongly in the ER of OE19 cells. In OE33 cells, AGR2 expression was only seen in a few cells and did not appear to show classical ER expression. This suggests that AGR2 expression may occur in OE33 cells but at a level that wasn't detectable in Western blotting. In OE19 cell lines AGR2 was shown to form high molecular weight disulphides, under non reducing conditions, in the presence of NEM. Further analysis of OE19 cells under redox conditions showed that the high molecular weight disulphides were redox dependant, suggesting that AGR2 may have a role in redox poise and perhaps oxidative protein folding in the ER of OE19 cells.

Discussion

7.1 Introduction

This study was based on the hypothesis that ER stress leads to the dysregulation of ER redox/protein folding networks in the oesophagus and that this ER dysregulation may play an important part in the disease BO and its transition to OAC.

Initial experiments focused on the proteins GPx7 and Prdx4 which play a role in both protein folding, via the ERO1-PDI pathway and in protecting the ER from ROS, a by-product of ERO1-PDI protein folding (Nguyen, et al., 2011) (Chen, et al., 2016). This was followed by the examination of AGR2, a member of the PDI family of proteins, which, due to its possible involvement in various cancers (Brychtova, et al., 2011), became a promising candidate for research into the transition of the oesophagus to BO and in some patients OAC.

Experimentally, some improvements could be made in the way the study was carried out to improve the weight of the results. The Western blotting experiments would benefit from more consistency, such that each blot should have followed the same format of reducing/non-reducing and +/-NEM. In addition each blot should have included PDI as a positive control and been re-probed with Actin

Similarly the controls for the Immunohistochemistry experiments could be improved. Initially pancreatic tissue was stained against insulin with an N90 antibody as a positive control. This should have been continued forward with all subsequent experiments. In relation to the AGR2 study, if the study was repeated, it would benefit from the inclusion of a negative control of to highlight any issues with overdevelopment. Suitable negative controls would be human tissue taken from the brain, muscle, adipose or skin which have low expression scores of AGR2, according to the Human Protein Atlas (Uhlen, et al., 2017)

7.2 The Expression of GPx7 in the ER, BO and OAC

GPx7 has a role as a scavenger of H_2O_2 in the ER and can utilise H_2O_2 in oxidative protein folding in consort with ERO1α and PDI (Nguyen, et al., 2011). Evidence from literature suggested that GPx7 may play a role in the pathogenesis of BO and OAC. Experiments with GPx7 had showed that it had a protective role in preventing oxidative DNA damage in oesophageal cells (Peng, et al., 2011) and that it had tumour suppressor capabilities which were down regulated in cancer cells by location specific methylation of the GPx7 promoter region (Peng, et al., 2014). Immunofluoresence of the cell lines HTL060, OE19, OE21 and OE33 showed some expression of GPx7 but this expression did not appear to be specifically localised to the ER when compared to PDI. In this thesis Western blotting of cell lysates taken from HTL060, OE19, OE21,OE33 and HeLa cells failed to show any expression of GPx7 at the expected molecular weight on the manufacturers data sheet. A likely non specific signal was seen in some experiments, for example in an OE33 cell lysate: but this signal was at a higher molecular weight than expected (Figure 4.2). The GPx7 antibody reactivity towards OE19 cell lysates were similar to the OE33 cell lysates, in that multiple bands could be seen at higher molecular weights but not at the expected molecular weight for GPx7. Considering the experimental data from both Western blotting and immunofluorescence together they seem to suggest that there was some non specific binding with the antibody and a lack of GPx7 expression. The likely lack of expression correlated well with the evidence that GPx7 is suppressed in cancer derived cell lines as described in the literature. Further experiments to determine the effects of ER stress on GPx7 expression would either require a transfection approach, the verification of GPx7 specific antibody, and/or a screen of cell lines to identify a cell type with high GPx7 levels which have

been suggested to express GP-7. For example, Peng *et al* had shown baseline expression of GP-7 in Western Blotting of BAR-T, HET-1-A, EPC2 and CP-A cells ((Peng, et al., 2011) supplementary data, figure 1)

Human tissue samples of BO and OAC were kindly provided by James Cook University Hospital and stained for GP-7 to determine if there was any correlation between tissue expression of GP-7 and the results seen in the cell line experiments. In the tissue samples of BO it appeared that GP-7 may be expressed in the lamina propria but there was no expression observed in the epithelial layer. In tissue taken from patients with OAC there appeared to be a small amount of expression which was located close but did not appear to be associated with tumour cells. Given the disordered nature of the tissue, expression could equally be from another cell type, such as gastric-like columnar cells rather than a tumour cell. *In situ* hybridisation or another complementary approach would be required to confirm GP-7 expression in this tissue.

GPx8 is homologous to GP-7 and merits further examination, in the context of this study. GPx8 is thought to perform a similar role to GP-7 in the ER, except that GP-7 is soluble in the ER lumen and GPx8 is membrane bound and localised to the inside of the ER membrane (Chen, et al., 2016). GPx8 has also been shown to have a higher expression level than GP-7 (Nguyen, et al., 2011). In tissue, GPx8 is expressed in the digestive system. The Human Tissue Atlas shows mixed, possibly tissue and/or antibody dependent, expression of GPx8 in the oesophagus and high expression in the stomach (Uhlen, et al., 2017). Therefore it may be possible compare any findings from the cell models to the disease.

If oxidative stress leads to redox dysfunction and dysregulation of the ER protein folding networks then, logically, something may also affect the H_2O_2 scavenging capacity of GPx8. As GPx8 performs a role in preventing the leakage of H_2O_2 from the ER (Rumming, et al., 2014) then dysfunction of GPx8 in BO could result in peroxide-induced DNA damage (Figure 7.1) and ultimately cause the transition from stable Barrett's to OAC.

Figure 7.1. Under normal conditions GPx8 prevents the leakage of H_2O_2 from the ER. The disruption of GPx8 would allow the leakage of H_2O_2 which could result in Oxidative DNA damage which may lead to changes in the cell which could cause the cell to become cancerous.

7.3 Expression of Prdx4

Like GPx7, Prdx4 is an H_2O_2 scavenger in the ER. Prdx4 can also aid in disulphide bond formation with PDI catalysing oxidative protein folding (Tavender, et al., 2008). It is thought that GPx proteins are the main removers of the excess H_2O_2 produced by oxidative protein folding in the ER and that Prdx4 only fulfils that role when levels of H_2O_2 are maximised (Rammog, et al., 2014). As such the study of Prdx4 becomes important in H_2O_2 given the evidence that GPx7 may be down regulated in BO (Peng, et al., 2014).

OE19 and OE33 cells were both shown to express Prdx4 by immunofluorescence and Western blot (Figure 5.3). There were observable differences in the expression of Prdx4 between OE33 and OE19 cells. In OE33 cells expression of Prdx4 seemed less tightly restricted to the ER then in OE19 cells. Western blotting of OE33 and OE19 lysates under reducing conditions showed expression of Prdx4 at the expected molecular weight and also showed bands at higher molecular weights suggesting that there may be a difference in redox poise between OE19 and "the more advanced" OE33 cells. Prdx4 has been shown to form decameric complexes (Tavender, et al., 2008), so under reducing conditions it is possible that the presence of NEM has trapped Prdx4 in a number of different states. Under non-reducing conditions, in the presence of NEM, Prdx4 may be trapped as a decamer. Interestingly there appeared to be a greater expression of Prdx4 in OE19 cell lysates compared to OE33 cell lysates, although whether the expression differences are reproducible requires further experiments. Both cell lines were originally derived from primary OAC tumour, with the OE19 cell line derived from a tumour at the oesophageal-gastric junction. While the OE33 cell line was originally derived from a tumour in the lower oesophagus with Barrett's metaplasia (Rockett JI, 1997). This

possibly suggests that cells located nearer the oesophageal-gastric junction, which would be more likely to experience an increased exposure to acid, may be more likely to express an increased Prdx6.

In human tissue sections stained for Prdx6, Prdx6 appeared to be expressed higher in normal gastric tissue than in normal oesophageal tissue. In stained samples of BO tissue Prdx6 expression did appear higher in areas containing gastric like cells compared to the areas containing squamous epithelium (Figure 5.4). This may possibly correlate with the differences observed between OE19 and OE33 cells which suggests that Prdx6 expression may be linked to the amount of gastric like cells in the area of BO.

Prdx6 expression in tissue taken from oesophageal gastric junction tumours differed between samples with some sections showing little to no expression of Prdx6 and some sections showing localised areas of staining in or near tumour cells. Prdx6 expression has been linked to a number of cancers. Prdx6 expression has been observed to be increased in areas of carcinoma, in breast and prostate cancers, compared to non-tumour tissue (Hess, et al., 2006). Similar increases in Prdx6 expression have also been found in Oral Cavity Squamous Cell Carcinoma and in Glioblastoma multiformes, an aggressive brain malignancy (Chang, et al., 2011) (Kim, et al., 2012). Additionally there is evidence that secreted Prdx6 may also be a factor in tumourgenesis. Secreted Prdx6 has been linked to cancer induced osteoclastogenesis (Rafiei, et al., 2015) suggesting that over expression of Prdx6 may be a factor in the transition of BO to OAC.

Immunohistochemistry, from the experiments, in this thesis, suggests that normal oesophageal expression of Prdx6 is low. It would be interesting to see if this is also

true in HET-1A or EPC2 cells. If so then it would be worthwhile subjecting those cell lines to stress e.g. peroxide and/or a bile acid cocktail alongside OE19 and OE33 cells to determine if they give the same response and to see if less or more stress is needed to cause Prdx4 expression to rise above baseline. Expression analysis could be done at both mRNA level and protein level. It may also be worth testing the media of the cell lines, particularly under stress conditions to see if any Prdx4 is secreted in response to stress conditions.

7.4 Expression of AGR2

AGR2 is an member of the PDI protein family. It is localised to the ER by a C-terminal KTEL motif, similar to the KDEL and KVEL ER retention sequences (Gupta, et al., 2012). Like PDI, AGR2 contains thioredoxin-like domain which could indicate a role for AGR2 in oxidative protein folding. However, unlike PDI, AGR2 contain a single redox active cysteine residue (Galligan & Peterson, 2012) suggesting that if it is involved in disulphide bond formation it may be via an unconventional route. Analysis by mass spectrometry has shown that AGR2 can dimerise by forming a disulphide bond with itself (Clarke, et al., 2016).

The experiments in Chapter 6, Figures 6.2 and 6.3, showed that AGR2 is expressed in both OE19 and OE33 cells. In OE19 cells AGR2 appears to be wholly expressed in the ER but in OE33 cells there was a suggestion that AGR2 was not wholly confined to the ER. There is evidence to suggest that AGR2s novel KTEL motif may allow it to be secreted (Fessart, et al., 2016) so it is plausible that, in OE33 cells, some AGR2 is secreted. Comparing OE19 cells and OE33 cells, AGR2 appeared to be more highly expressed in the OE19 cell line than in OE33 cells. Western blot

analysis of lysates taken from OE19 and OE33 cells appear to support this where AGR2 was detected in OE19 lysates but not in OE33 cells in reduced samples.

Further examination of AGR2 expression in OE19 lysates showed clearly that, under non reducing conditions, AGR2 can form a dimer. In addition detection of multiple bands in non reduced samples, in the presence of NEM, suggest that AGR2 is also capable of binding to other proteins reinforcing the idea that AGR2 may be involved in the in protein folding. Further experiments support this assertion, for example the treatment of OE19 cells with DTT showed a reduction of all AGR2 client interactions, including the reduction of dimers to monomers. A DTT washout and recovery experiment showed that after recovery the AGR2 dimer and other AGR2 protein interactions returned to the control status (Figure 6.4). Diamide cause an increase in AGR2 client interactions which, when allowed to recover, returned towards baseline expression. This evidence clearly indicates that AGR2 client protein is redox dependant and that AGR2 interactions are occuring through disulphide bond formation.

Evidence in the literature suggests that AGR2 interacts with BiP/Grp78 (Ryu, et al., 2013). Going forward it would be helpful to identify the AGR2 client protein parameters using mass spectrometry to first determine possible interactions before conducting further co-immunoprecipitation experiments.

AGR2 expression levels are also associated with various cancers, in particular hormone dependant breast and prostate cancer and in hormone independent colorectal, pancreatic and gastric cancers (Brychtova, et al., 2011). Due to AGR2's association with cancer it was worth investigating if AGR2 had any role in BO and OAC. Experiments with normal oesophageal and normal gastric tissue showed that

AGR2 was not expressed in the normal oesophagus. AGR2 was found to be expressed at low levels in normal gastric tissue in the secretory of the gastric cardia. AGR2 has a role in mucus production particularly the MUC2 mucin in the intestines (Bergstrom, et al., 2014) (Park, et al., 2009) and in MUC1 and MUC5AC (Patel, et al., 2013), so its presence in the normal gastric samples was anticipated. In BO there is an associated change in the morphology of the epithelium of the distal oesophagus, where the stratified squamous epithelium is replaced with a metaplastic columnar epithelium of mixed morphologies (di Pietro, et al., 2014). Sections taken from human patients with BO showed a great variation in the morphology of the cell types between sections (Figure 6.1.C and D). Examination of AGR2 expression in these sections showed expression of AGR2 in areas where the morphology had changed to simple columnar epithelium and to areas of gland like tissue. Expression appeared particularly high in the areas resembling gastric secretory cells suggesting that these cells may be expressing higher levels of AGR2 than those present in the normal gastric epithelium. Although not tested it would be particularly interesting to examine if these gastric-like secretory cells were also expressing any mucins. If this was found to be true it would agree in part that the morphological changes present in BO may indeed be a protective adaptation to increased acid secretion from GORD (Ostowski, et al., 2007). Further a recent paper by Jiang *et al* suggest that AGR2 positive secretory like cells may centrally involved in the transition to BO at the gastro-oesophageal junction (Jiang, et al., 2017).

Examination of AGR2 expression in OAC taken from patients with oesophageal junction tumours showed high expression of AGR2 in areas of secretory-like tissue in the same way as those in the BO tissue sections. There appeared to be no expression of AGR2 in the areas of oesophageal tumour, but those cells expressing

AGR2 cells appeared adjacent to the tumour cells. Experiments with PDAC found that discrete subpopulation of AGR2 expressing cells were present neighbouring pre-neoplastic lesions (Dumartin,et al., 2010). In a similar way it could be possible that secretion of AGR2 may be a factor in the transformation of BO to OAC.

It would be useful to stain further samples taken from patients, particularly a series of experiments on tissue samples taken from the same patients pre-BO and with-BO to see if the apparent difference in expression of AGR2 between pre-BO and BO holds. In addition, it would be useful to examine those patients who have stable-BO and those where BO develops into OAC to see if the tumours are neighbouring AGR2 expressing cells. It would be also useful to try to determine if there is a tissue association between AGR2 and mucin production either by co-staining for mucin or in situ hybridisation for AGR2 and the various MUC genes using different fluorescent tags or stains.

It would also be useful to examine whether stress effects AGR2 expression in OE19 cells in culture. Evidence from Clarke *et al* suggests that AGR2 dimerisation occurs through a sulphenic acid intermediate and that high concentrations of H_2O_2 inhibits dimer formation (Clarke, et al., 2010). It would therefore be useful to titrate different concentrations H_2O_2 to examine AGR2 expression and dimer formation to see if this is the case in OE19 cells. In addition it would also be beneficial to expand this approach to include other reducing and stress-inducing agents, such as tunicamycin which induces ER stress.

7.6 Conclusions

The overall aim of this thesis, was to examine the effects of stress inducing agents on chaperone interactions using oesophageal cell lines as a cellular model of BO, focusing initially on GPx7 and Prdx4. This thesis found that GPx7 was not expressed or not expressed at sufficient levels to be detected in the oesophageal cell lines tested but that Prdx4 was expressed in OE19 cells and could be detected with the Prdx4 [TA313/16943] antibody (Abcam). However, further experiments are required to validate GPx7 expression levels with other. Considering AGR2, this thesis has shown that AGR2 is not expressed in the normal oesophagus but is expressed in BO. Furthermore AGR2 is associated closely with tumour cells in OAC (Figure 6.1 E and F). In OE19 cells AGR2 was shown to form redox dependant dimers as well as interactions with other, as yet unknown, proteins. This suggests that AGR2 plays role in the pathogenesis of OAC and may be an important factor in the transition of BO to OAC, with the mechanism still to be determined.

Bibliography

Abcam, 2017. *BioPorato Anti-Glutathione Peroxidase 7 antibody [2F5d]*. [Online] Available at: http://www.bioprofitub.com/Antibodies/108410-anti-glutathione-peroxidase-7-antibody-2f5d?filename=bio_genes [Accessed 30 April 2017].

Aberger, F., Weidinger, G., Grunz, H. & Richter, K., 1998. Anterior specification of embryonic ectoderm: the role of the Xenopus cement gland-specific gene XAG-2. *Mech Dev*, Volume 70, pp. 115-130. DOI:10.1016/S0925-4773(97)00331-x

Battle, D. M. et al., 2013. Expression of the Endoplasmic Reticulum Oxidoreductase Ero1a in Gastro-Intestinal Cancer Reveals a Link Between Homocysteine and Oxidative Protein Folding. *Antioxidants & Redox Signalling*, 19(1). DOI:10.1089/ars.2012.4601

Benham, A. M., 2012. The Protein Disulphide Family: Key Players in Health and Disease. *ANTIOXIDANTS & REDOX SIGNALING*, 16(8), pp. 781-789. DOI:10.1089/ars.2011.4439

Benham, A. M. et al., 2008. The C-XXC-XXC motif determines the folding, structure and stability of human Ero1alpha. *EMBO J*, Volume 16, pp. 4460-4510. DOI:10.1038/emboj.2013.17.4458

Bergstrom, J. H. et al., 2014. AGR2, an Endoplasmic Reticulum Protein, Is Secreted into the Gastrointestinal Mucus. *Plos one*, 9(8). DOI: 10.1371/journal.pone0104198

Bernstein, H. et al., 2005. Bile acids as carcinogens in human gastrointestinal cancers. *Mutation Research*, Volume 589, pp. 47-65. DOI:10.1016/j.mrrev.2004.09.001

Bernstein, H., Bernstein, C., Payne, C. M. & Dvorak, K., 2009. Bile acids as endogenous etiologic agents in gastrointestinal cancer. *World J Gastroenterol*, 15(27), pp. 3329-3340. DOI:10.3748/wjg.15.3329

Bernstein, H. et al., 1999. Activation of the promoters of genes associated with DNA damage, oxidative stress, ER stress and protein malfolding by the bile salt, deoxycholate. *Toxicology Letters*, Volume 108, pp. 37-46.

Braakman, I. & Bulleid, N. J., 2011. Protein Folding and Modification in the Mammalian Endoplasmic Reticulum. *Annual Reviewt in Biochemistry*, Volume 80, pp. 9.1-9.26. DOI: 10.1146/annurev-biochem-062209-093836

Brown, H., 2002. *www.umd.edu*. [Online] Available at: http://www.umd.edu/dept/cmns/2007fallbrown/635/635.Primer.HallGrant04.pdf [Accessed 6-8 2017].

Brychtova, V., Vojtesek, B. & Hrstka, R., 2011. Anterior gradient 2: A novel player in tumor cell biology. *Cancer Letters*, Volume 304, pp. 1-7. DOI: 10.1016/j.canlet.2010.12.020

Brychtova, V., Mohtar, A., Vojtesek, B. & Hupp, T. R., 2015. Mechanisms of anterior-gradient-2 regulation and function in cancer. *Seminars in Cancer Biology*, Volume 33, pp. 16-24. DOI: 10.1016/j.semcancer.2015.04.005

Bu, H. et al., 2013. Anterior gradient 2 and 3 – two prototype androgen-responsive genes transcriptionally upregulated by androgens and by oestrogens in prostate cancer cells. *FEBBS Journal*, 280(9), pp. 1248-1266. DOI: 10.1111/febs.12116 &pub.1013/Feb13

Bulleid, N. J., 2012. Disulfide Bond Formation in the Mammalian Endoplasmic Reticulum. *Cold Spring Harbour Perspectives in Biology*, Volume 4:a013219. DOI:10.1101/cshperspect.a013219

Bulleid, N. & Jessop, C., 2004. Glutathione directly reduces an oxidoreductase in the endoplasmic reticulum of mammalian cells. *J Biol Chem*, 279(32), pp. 33241-7. DOI:10.1074/jbc.M314459200

Bulleid, N. J. & Ellgaard, L., 2011. Multiple ways to make disulphides. *Trends in Biochemical Sciences*, 36(9), pp. 485-492. DOI:0.1016/j.tibs.2011.06.004

Burke, Z. & Tosh, D., 2012. Barrett's Metaplasia as a paradigm for understanding the development of cancer. *Current Opinion in Genetics and Development*, Volume 22, pp. 494-499. DOI:10.1016/j.gde.2010.08.001

Burton, G. J. & Jauniaux, E., 2010. Oxidative Stress. *Best Practice & Research Clinical Obstetrics and Gynaecology*, Volume 25, pp. 287-299. DOI:10.1016/j.bpobgyn.2010.10.016

Chakravarthi, S., Jessop, C. E. & Bulleid, N. J., 2006. The role of glutathione in disulphide bond formation and endoplasmic reticulum-generated oxidative stress. *EMBO reports*, 7(3), pp. 271-275. DOI:10.1038/sj.embor.7400645

Chakravarthi, S. et al., 2007. Intracellular catalysis of disulfide bond formation by the human sulfhydryl oxidase QSOX1. *Biochem J*, 404(PtO), pp. 403-411. DOI:10.1042/BJ20061510

Chang, K. et al., 2011. Identification of PRDX4 and P4HA2 as Metastasis-Associated Proteins in Oral Cavity Squamous Cell Carcinoma by Comparative Tissue Proteomics of Microdissected Specimens Using ITRAQ Technology. *Journal of Proteome Research*, 10(11), pp. 4935-4947. DOI:10.102/pr200931p

Chen, Y. et al., 2016. NPGPx (GPx7): a novel oxidative stress sensor/transmitter with multiple roles in redox homeostasis. *Am J Transl Res*, 8(4), pp. 1636-1640.

Clarke, D. J. et al., 2014. Mass spectrometry analysis of the oxidation states of the pro-oncogenic protein anterior gradient-2 reveals covalent dimerization via an intermolecular disulphide bond. *Biochimica et Biophysica Acta*, Volume 1844, pp. 861-941. DOI:10.1016/j.bbapap.2014.02.014

Desilva, M., Norbeis, A. & Lan, M., 1997. Molecular characterization of a pancreas-specific protein disulfide isomerase, PDIp.. *DNA Cell Biol*, 16(3), pp. 269-74. 1 DOI:0.1089/dna.1997.16.269

Devaraneni, P. K. et al., 2011. Stepwise insertion and inversion of a type II signal anchor sequence in the ribosome-Sec61 translocon complex. *Cell*, Volume 146, pp. 134-147. DOI:10.1016/j.cell.2011.06.004

di Pietro, M., Alzoubaidi, D. & Fitzgerald, R., 2014. Barrett's Esophagus and Cancer Risk: How Research Advances Can Impact Clinical Practice. *Gut and Liver*, 8(4), pp. 356-370. DOI:10.5009/gnl.2014.8.4.356

Dicomenod, J. et al., 2004. Differential downregulation of endoplasmic reticulum-residing chaperones calnexin and calreticulin in human metastatic melanoma. *Cancer Letters*, 203(2), pp. 221-231. DOI:10.1016/j.canlet.2003.09.026

Dumartin, L. et al., 2011. ER stress protein AGR2 precedes and is involved in the regulation of pancreatic cancer initiation. *Oncogene*, pp. 1-10. DOI:10.1038/onc.2010.459

Dvorak, K. et al., 2007. Bile acids in combination with low ph induce oxidative DNA damage: relevance to the pathogenesis of Barrett's Oesophagus. *Gut*, Volume 56, pp. 763-771. DOI:10.1136/gut.2006.103887

Ellgaard, L. & Frickel, E., 203. Calnexin, Calreticulin and ERp57 Teamates in Glycoprotein Folding. *Cell Biochemistry and Biophysics*, Volume 39, pp. 223-247. DOI:10.1385/CBB:39:3:223

English, A. R. & Voeltz, G. K., 2013. Endoplasmic Reticulum Structure and Interconnections with Other Organelles. *Cold Spring Harbour Perspectives in Biology*, 5(4):a013227. DOI:10.1101/cshperspect.a013227

Fass, R. et al., 2001. Correlation of Oesophageal Acid Exposure with Barrett's Oesophagus Length. *Gut*, Volume 48, pp. 310-313. DOI:10.1136/gut.48.3.310

Fessart, D. et al., 2016. Secretion of protein disulphide isomerase AGR2 confers tumorigenic properties. *eLIFE*, Volume 5. DOI:10.7554/eLife.13497

Fletcher, G. C. et al., 2003. hAG-2 and hAG-3, human homologues of genes involved indifferentiation, are associated with oestrogen receptor positive breast tumours and interact with metastatic gene C4.4a and dystroglycan. *Brit. J. Cancer*, Volume 88, pp. 579-585. DOI:10.1038/sj.bjc.6600743

Fujimura, T. et al., 2011. nflammation-Related Carcinogenesis and Prevention in Esophageal Adenocarcinoma Using Rat Duodenoesophageal Reflux Models. *Cancers*, 3(3), pp. 3206-3224. DOI:10.3390/cancers3033206

Galligan, J. & Petersen, D., 2012. The human protein disulfide isomerase gene family. *Human Genomics*, 6(6). DOI:10.1186/1479-7364-6-6

Gatenby, P. & Soon, Y., 2014. Barrett's oesophagus: Evidence from the current metaphylaxes. *World Journal of Gastrointestinal Pathophysiol*, 5(3), pp. 178-187. DOI:10.4291/wjgp.v5.i3.178

Gunasekara, S. D., 2004. *Characterising the expression and interactions of the Endoplasmic Reticulum Oxidoreductase Ero1ß*. Durham, United Kingdom: University of Durham.

Gupta, A., Dong, A. & Lowe, A. W., 2012. AGR2 Gene Function Requires a Unique Endoplasmic Reticulum Localization Motif. *JBC*, 287(7), pp. 4773-4782. DOI:10.1074/jbc.M111.301531

Hainzl, T. et al., 2011. Structural basis of signal-sequence recognition by the signal recognition particle. *Nature Structural Molecular Biology*, Volume 18, pp. 389-391. DOI:10.1038/nsmb.1994.Epub.2011Feb20

Heijne, G. v., 1985. Signal Sequences: The limits of variation. *Journal of Molecular Biology*, Volume 184, pp. 99-105.

Helenius, A., Trombetta, E. S., Hebert, D. N. & Simons, J. F., 1997. Calnexin, Calreticulin and the Folding of Glycoproteins. *trends in Cell Biology*, Volume 7, pp. 193-200. DOI:10.1016/S0962-8924(97)01032-4

Hess, K. R. et al., 2006. Metastatic Patterns in Adenocarcinoma. *Cancer*, 106(7), pp. 1624-1633. DOI:10.1002/cncr.21778

Higa, A. et al., 2011. Role of Pro-oncogenic Protein Disulfide Isomerase (PDI) Family Member Anterior Gradient 2 (AGR2) in the Control of Endoplasmic Reticulum Homeostasis. *J. Biol Chem*, Volume 286, pp. 44655-44649. DOI:10.1074/jbc.M110.2701139

Huo, Y. et al., 2011. Deoxycholic acid causes DNA damage while inducing apoptotic resistance through NF-κB activation in benign Barrett's epithelial cells. *Am J Physiol Gastrointestinal and Liver Physiology*, 301(23), pp. G278-G286. DOI:10.1152/ajpgi.00092.2011

Ikawa, M. et al., 2011. Calsperin is a testis-specific chaperone required for sperm fertility.. *J Biol Chem*, 286(7), pp. 5039-46. DOI:10.1074/jbc.M110.141523.Epub.2010Dec3

Jiang, M. et al., 2017. Transitional basal cells at the squamous–columnar junction generate Barrett's oesophagus. *Nature*, Volume 550. DOI:10.1038/nature24289

Kabbage, M. et al., 2013. Calreticulin expression in infiltrating ductal breast carcinomas: relationships with disease progression and humoral immune responses. *Tumor Biology*, Volume 34, pp. 1177-1186. DOI:10.1007/s13277-013-0661-y

Kershaw, S., 2004. The Gastrointestinal System at a Glance. Massachusetts: Blackwell Science Ltd

Kim, T. H. et al., 2012. Suppression of Peroxiredoxin 4 in Glioblastoma Cells Increases Apoptosis and Reduces Tumor Growth. *PLOS one*, 7(8). DOI:10.1371/journal.pone.0042816

Langer, R. et al., 2008. Expression and clinical significance of Glucose-Regulated Proteins GRP78/BiP1 and GRP94/GP96) in human adenocarcinomas of the esophagus. *BMC Cancer*, 8(73). DOI:10.1186/1471-2407-8-73

Lee, D. et al., 2005. Hypermethylation and Loss of Expression of Glutathione Peroxidase-3 in Barrett's Tumorigenesis. 7(9), pp. 854-860. DOI:10.1593/neo.05328

Levine, D. et al., 2013. A Genome-wide Association Study Identifies New Susceptibility Loci for Esophageal Adenocarcinoma and Barrett's Esophagus. *Nature Genetics*, 45(12). DOI:10.1038/ng.2796

Leydold, S. M. et al., 2011. Peroxiredoxin-4 Is Over-Expressed in Colon Cancer and Its Down-Regulation Leads to Apoptosis. *Cancer Growth and Metastasis*, Volume 7, pp. 7-23. DOI:10.4137/CGM.S6584

Mendez, M. 2016. *simple.wikipedia.org*.\[Online] Available at: https://simple.wikipedia.org/wiki/Endoplasmic_reticulum#/media/File:Nuclear_ER_gold.jpg \[Accessed 16 02 2017].

McCullough, K. D. et al., 2001. Gadd153 Sensitizes Cells to Endoplasmic Reticulum Stress by Down-Regulating Bcl2 and Perturbing the Cellular Redox State. *Molecular and Cellular Biology*, 21(4), pp. 1249-1259. DOI:10.1128/MCB.21.4.1249-1259.2001

Munro, S. & Pelham, H. R., 1987. A C-Terminal Signal Prevents Secretion of Luminal ER Proteins. *Cell*, Volume 48, pp. 899-907.

Ng, D. T. & Walter, P., 1996. Protein translocation across the endoplasmic reticulum. *Current Opinion in Cell Biology*, Volume 6, pp. 510-516.

Nguyen, V. D. et al., 2011. Two Endoplasmic Reticulum PDI Peroxidases Increase the Efficiency of the Use of Peroxide during Disulfide Bond Formation. *J Mol Biol*, Volume 406, pp. 503-515. DOI:10.1016/j.jmb.2010.12.039

Nyathi, Y., Wilkinson, B. M. & Pool, M. R., 2013. Co-translational targeting and translocation of proteins to the endoplasmic reticulum. *Biochimi et Biophysica Acta - Molecular Cell Research*, 1833(11), pp. 2392-2402. DOI:10.1016/j.bbamcr.2013.02.021."2013"

Omikorede, O. et al., 2013. ER stress in rodent islets of Langerhans is concomitant with obesity and β-cell compensation but not with β-cell dysfunction and diabetes. *Nutr Diabetes*, 3(10). DOI:10.1038/nutd.2013.35

O'Riordan, J. M. et al., 2005. Proinflammatory Cytokine and Nuclear Factor Kappa-B Expression along the Inflammation-Metaplasia-Dysplasia-Adenocarcinoma Sequence in the Esophagus. *American Journal of Gastroenterology*, Volume 100, pp. 1257-1264. DOI:10.1111/j.1572-0241.2005.41338.x

Ostowski, J. et al., 2007. Molecular defence mechanisms of Barrett's metaplasia estimated by its integrative genomics. *J Mol Med (Berl)*, 85(7), pp. 733-43. DOI:10.1007/s00109-007-0178-9

Pagani, M. et al., 2000. Endoplasmic reticulum oxidoreductin 1-Lβ (ERO1-Lβ), a human gene induced in the course of the unfolded protein response. *J Biol Chem*, Volume 275, pp. 23685-23692. DOI:10.1074/jbc.M909382200

Park, S. et al., 2009. The protein disulfide isomerase AGR2 is essential for production of intestinal mucus. *PNAS*, 106(17), pp. 6950-6955. DOI:10.1073/pnas.0808723106

Patel, P. et al., 2013. Metastasis-Promoting Anterior Gradient 2 Protein Has a Dimeric Thioredoxin Fold Structure and a Role in Cell Adhesion. *J Mol Biol*, Volume 425, pp. 628-643. DOI:10.1016/j.jmb.2012.09–Dec-08

Peng, D. et al., 2012. Glutathione peroxidase 7 protects against oxidative DNA damage in oesophageal cells. *Gut*, Volume 61, pp. 1250-1260. DOI:10.1136/gutjnl-2011-301078

Peng, D. et al., 2014. Glutathione peroxidase 7 has potential tumour suppressor functions that are silenced by location-specific methylation in oesophageal adenocarcinoma. *Gut*, Volume 63, pp. 549-561. DOI:10.1136/gutjnl-2012-304069

Peng, D. et al., 2014. Loss of glutathione peroxidase 7 promotes TNF-α-induced NF-κB activation in Barrett's carcinogenesis. *Carcinogenesis*, 35(7), pp. 1620-1628. DOI:10.1093/carcin/bgu083

Persson, S. et al., 2005. Diversity of the protein disulfide isomerase family: Identification of breast tumor induced Hag2 and Hag3 as novel members of the protein family. *Molecular Phylogenetics and Evolution*, Volume 36, pp. 738-748. DOI:10.1016/j.ympev.2005.04.02

Pohler, E. et al., 2004. The Barrett's Antigen Anterior Gradient-2 Silences the p53 Transcriptional Response to DNA Damage. *Mol. Cell Proteomics*, Volume 3, pp. 534-547. DOI:10.1074/mcp.M500069-MCP200

Pool, M. R., 2005. Signal recognition particles in chloroplasts, bacteria, yeast and mammals. *Molecular Membrane Biology*, 22(1-2), pp. 3-15.

Quante, M. et al., 2012. Bile Acid and Inflammation Activate Gastric Cardia Stem Cells in a Mouse Model of Barrett-Like Metaplasia. *Cancer Cell*, Volume 21, p. 36=51. DOI:10.1016/j.ccr.2011.12.004

Radisi, S. et al., 2015. Peroxiredoxin 4: A novel secreted mediator of cancer induced osteoclastogenesis. *Cancer Letters*, Volume 366, pp. 262-270. DOI:10.1016/j.canlet.2015.03.012

Ramming, T. et al., 2014. GPx8 peroxidase prevents leakage of H2O2 fromthe endoplasmic reticulum. *Free Radical Biology and Medicine*, Volume 70, pp. 106-116. DOI:10.1016/j.freeradbiomed.2014.01.018

Ramming, T. et al., 2015. A PDI-catalyzed thiol-disulfide switch regulates the production of hydrogen peroxide by human GPX1. *Free Radical Biology and Medicine*, Volume 86, pp. 361-372. DOI:10.1016/j.freeradbiomed.2015.02.011

Rasheed, S. et al., 1974. Characterization of a newly derived human sarcoma cell line (HT-1080). *. Cancer*, 4(April3), pp. 1027-33.

Rockett, J et al., 1987. Five newly established oesophageal carcinoma cell lines: phenotypic and immunological characterization.. *Br J Cancer* , 75(3), pp. 358-263.

Ross-Innes, C. S. et al., 2015. Whole-genome sequencing provides new insights into the clonal architecture of Barrett's esophagus and esophageal adenocarcinoma. *Nature Genetics*, Volume 9, p. 47. DOI:10.1038/ng.3157

Ryner, S. et al., 2011. Gene expression profiling of rat spermatogonia and Sertoli cells reveals signaling pathways from stem cells to niche and testicular cancer cells to surrounding stroma. *BMC Genomics*, 12(29), pp. 1-16. DOI:0.1186/1471-2164-12-29

Ryu, J. et al., 2012. Dimerization of pro-oncogenic protein Anterior Gradient 2 is required for the interaction with BiP/GRP78. *Biochemical and Biophysical Research Communications*, Volume 430. pp. 610-615. DOI:10.1016/j.bbrc.2012.11.05

Sarosi, G. et al., 2008. Bone marrow progenitor cells contribute to esophageal regeneration and metaplasia in a rat model of Barrett's esophagus. *Diseases of the Esophagus*, Volume 21. pp. 49-53. DOI:10.1111/j.1442-2050.2007.00741

Scherer W., S. J. G. G., 1953. STUDIES ON THE PROPAGATION IN VITRO OF POLIOMYELITIS VIRUSES IV. VIRAL MULTIPLICATION IN A STABLE STRAIN OF HUMAN MALIGNANT EPITHELIAL CELLS (STRAIN HELA) DERIVED FROM AN EPIDERMOID CARCINOMA OF THE CERVIX. *J Exp Med*, May 1,96(5). pp. 695-710.

Schroder, M. & Kaufman, R. J., 2005. ER stress and the unfolded protein response. *Mutation Research*, Volume 569. pp. 29-63. DOI:10.1016/j.mrfmmm.2004.06.056

Schwartz, T. & Blobel, G., 2003. Structural basis for the function of the beta subunit of the eukaryotic signal-receptor particle. *Cell*, Volume 112. pp. 793-803. DOI: 10.1016/S0092-8674(03)00183-3

Schwarz, D. S. & Blower, D. M., 2016. The Endoplasmic Reticulum: structure, function and response to cellular signalling. *Cellular and Molecular Life Sciences*, Volume 73. pp. 79-94. DOI10.1007/s00018-015-2052-6

Sevier, C. S. & Kaiser, C. A., 2008. ERO1 and redox homeostasis in the endoplasmic reticulum. *Biochimica et Biophysica Acta - Molecular Cell Research*, 1783(4). pp. 549-556. DOI:10.1016/j.bbamcr.2007.12.011

Shaw, A. E., Rotter, P. J. & Rose, J. K., 1988. Evidence for the loop model of signal sequence insertion into the endoplasmic reticulum. *Proc Nat Acad Sci USA*, Volume 85. pp. 7843-7846.

Sheykhkhi, L. Hasini, A., Zheng, F. & Ma, H., 2014. Epigenetic Changes within the Promoter Regions of Antigen Processing Machinery Family Genes in Kazakh Primary Esophageal Squamous Cell Carcinoma. *Asian Pacific Journal of Cancer Prevention*, Volume 15. pp. 10299-10306. DOI:10.7314/APJCP.2014.15.23.10299

Spechler, S. & Souza, R., 2014. Barrett's Esophagus. *NewEngland Journal of Medicine*, 371(9). pp. 836-845. DOI:10.1056/NEJMra1314704

Stachler, M. D. et al., 2015. Paired exome analysis of Barrett's esophagus and adenocarcinoma. *Nature genetics*, 47(9). pp. 1047-1055. DOI:10.1038/ng.3343

Stevens, A. & Lowe, J., 1997. *Human Histology*. 2nd ed. London: Mosby.

Tavender, T. J., Sheppard, A. M. & Bulleid, N. J., 2008. Peroxiredoxin IV is an endoplasmic reticulum-localized enzyme forming oligomeric complexes in human cells. *Biochem J*, Volume 411. pp. 191-199. DOI:10.1042/BJ20071518

Tavender, T. J., Springate, J. J. & Bulleid, N. J., 2010. Recycling of peroxiredoxin IV provides a novel pathway for disulphide formation in the endoplasmic reticulum. *The EMBO Journal*, Volume 29. pp. 4185-4197. DOI:10.1038/emboj.2010.272

Terezaki, M. et al., 2013. Stacked endoplasmic reticulum sheets are connected by helicoidal membrane motifs. Cell, 154(2), pp. 285-296. DOI:10.1016/j.cell.2013.06.031

The Esophageal Adenocarcinoma Genetics Consortium and the Wellcome Trust Case Control Consortium , 2012. Common variants at the MHC locus and at chromosome 16q24.1 predispose to Barrett's esophagus. Nature Genetics, 44(3), pp. 1131-11-36. DOI:10.1038/ng.1408

To, H. et al., 2016. The Genetics of Barrett's Esophagus: A Familial and Population Based Perspective. Dig Dis Sci, Volume 61, pp. 1826-1834. DOI:10.1007/S10620-016-4109-2

Tsotakos, C. et al., 2000. Tumour necrosis factor-α in Barrett's oesophagus: a potential bowel mechanism of action. Oncogene, Volume 21, pp. 6071-6081. DOI:10.1038/sj.onc.1205731

Uhlen, M. et al., 2017. *The Human Protein Atlas*. [Online]
Available at: https://www.proteinatlas.org/ENSG00000178318-CALR/tissue/pancreas
[Accessed 10 08 2017].

Walter, P. & Blobel, G., 1983. Disassembly and reconstruction of signal recognition particle. Cell, Volume 34, pp. 525-533.

Wang, D. et al., 2010. Aberrant Epithelial-Mesenchymal Hedgehog Signalling Characterizes Barrett's Metaplasia. *Gastroenterology*, 138(5), pp. 1810-1822. DOI:10.1053/j.gastro.2010.01.049

Wang, H. et al., 2009. TNF-related apoptosis-inducing ligand suppresses PRDX4 expression. *FEBS Letters*, Volume 583, pp. 1511-1515. DOI:10.1016/j.febslet.2009.04.009 Epub 2009/Apr/21

Wang, L. et al., 2014. Glutathione Peroxidase 7 Utilizes Hydrogen Peroxide Generated by Ero1α to Promote Oxidative Protein Folding. *Antioxidants & Redox Signalling*, 20(4), pp. 545-557. DOI:10.1089/ars.2013.5236

Wang, X. et al., 2011. Residual Embryonic Cells as Precursors of a Barrett's-like Metaplasia. Cell, Volume 145, pp. 1023-1035. DOI:10.1016/j.cell.2001.05.036

Wang, X. et al., 2012. Structural insights into the peroxidase activity and inactivation of human peroxiredoxin 4. *Biochem J*, Volume 441, pp. 113-118. DOI:10.1042/BJ20110360

Watson, A., 2014. *UK Barrett's Oesophagus Registry*. [Online]
Available at: https://www.wonca.net/documents/Publications/Journal/Health-professionals-UK-Barretts-Oesophagus-Registry%20aspx#UKchangedt-UK-Barretts-Oesophagus-Registry
[Accessed 10 10 2016].

Watson, A. & Galloway, J., 2014. Heartburn, Barrett's Oesophagus and Cancer: Implications for Primary Care. *British Journal of General Practice*, pp. 120-121. DOI:10.3399/bjgp.14X677380

Zamanian, M. et al., 2016. Calreticulin mediates an invasive breast cancer phenotype through the transcriptional dysregulation of p53 and MAPK pathways. *Cancer Cell International*, 16(54). DOI:10.1186/S12935-016-0329-y

Zhang, H. Y. et al., 2009. In Barrigo Barrett's Epithelial Cells, Acid Exposure Generates Reactive Oxygen Species that Cause DNA Double-Strand Breaks. *Cancer Res*, 69(23), pp. 9083-9089. DOI:10.1158/0008-5472.CAN-09-2158

Zhang, K., 2010. Integration of ER stress, oxidative stress and the inflammatory response in health and diseases. *Int J Cell Exp Med*, 2(1), pp. 19-48. Published online 2010 Jan 8

Zhang, X., Rechtl, R., Wang, K. & Shan, S. O., 2010. Sequential checkpoins govern substrate selection during cotranslational protein targeting. *Science*. Volume 328, pp. 757-760. DOI:10.1126/science.1188743

Zhao, F. et al., 2010. Disruption of Paneth and goblet cell homeostasis and increased endoplasmic reticulum stress in Agr2−/− mice. *Dev Biol*. 338(2), pp. 270-276 DOI:10.1016/j.ydbio.2009.12.008

Zimmermann, R., Eyrisch, S., Ahmad, M. & Helms, V., 2011. Protein translocation across the ER membrane. *Biochimica et Biophysica Acta*. Volume 1808, pp. 912-924. DOI:10.1016/j.bbamem.2010.08.015

Zweitzig, D. R. et al., 2007. Physiological stress induces the metastasis marker AGR2 in breast cancer cells. *Mol Cell Biochem*. Volume 306, pp. 259-263. DOI:10.1007/S11010-007-9562-y